



**HAL**  
open science

# Late Miocene Intensified Tectonic Uplift and Climatic Aridification on the Northeastern Tibetan Plateau: Evidence From Clay Mineralogical and Geochemical Records in the Xining Basin

Rongsheng Yang, Yibo Yang, Xiaomin Fang, Xiaobai Ruan, Albert Galy, Chengcheng Ye, Qingquan Meng, Wenxia Han

## ► To cite this version:

Rongsheng Yang, Yibo Yang, Xiaomin Fang, Xiaobai Ruan, Albert Galy, et al.. Late Miocene Intensified Tectonic Uplift and Climatic Aridification on the Northeastern Tibetan Plateau: Evidence From Clay Mineralogical and Geochemical Records in the Xining Basin. *Geochemistry, Geophysics, Geosystems*, 2019, 20 (2), pp.829-851. 10.1029/2018GC007917 . hal-03407961

**HAL Id: hal-03407961**

**<https://hal.science/hal-03407961v1>**

Submitted on 20 Dec 2021

**HAL** is a multi-disciplinary open access archive for the deposit and dissemination of scientific research documents, whether they are published or not. The documents may come from teaching and research institutions in France or abroad, or from public or private research centers.

L'archive ouverte pluridisciplinaire **HAL**, est destinée au dépôt et à la diffusion de documents scientifiques de niveau recherche, publiés ou non, émanant des établissements d'enseignement et de recherche français ou étrangers, des laboratoires publics ou privés.

Copyright

# Geochemistry, Geophysics, Geosystems

## RESEARCH ARTICLE

10.1029/2018GC007917

### Key Points:

- A long-term gradual aridification since 12.7 Ma and an enhanced drying event since ~7.8 Ma occurred in the Xining Basin
- Uplift of the northeastern Tibetan Plateau was the major driver of the evolution of regional climate and landscape since the late Miocene
- Clay minerals are well-used potential proxies for paleoclimatic reconstructions in complex sedimentary routing systems

### Supporting Information:

- Supporting Information S1
- Data Set S1

### Correspondence to:

X. Fang,  
fangxm@itpcas.ac.cn

### Citation:

Yang, R., Yang, Y., Fang, X., Ruan, X., Galy, A., Ye, C., Meng, Q., & Han, W. (2019). Late Miocene intensified tectonic uplift and climatic aridification on the northeastern Tibetan Plateau: Evidence from clay mineralogical and geochemical records in the Xining Basin. *Geochemistry, Geophysics, Geosystems*, 20, 829–851. <https://doi.org/10.1029/2018GC007917>



Received 20 AUG 2018

Accepted 14 JAN 2019

Accepted article online 17 JAN 2019

Published online 7 FEB 2019

## Late Miocene Intensified Tectonic Uplift and Climatic Aridification on the Northeastern Tibetan Plateau: Evidence From Clay Mineralogical and Geochemical Records in the Xining Basin

Rongsheng Yang<sup>1,2,3</sup> , Yibo Yang<sup>1,4</sup> , Xiaomin Fang<sup>1,4,2</sup> , Xiaobai Ruan<sup>1,2,3</sup>, Albert Galy<sup>3</sup> , Chengcheng Ye<sup>1</sup>, Qingquan Meng<sup>5</sup> , and Wenxia Han<sup>6</sup>

<sup>1</sup>Key Laboratory of Continental Collision and Plateau Uplift, Institute of Tibetan Plateau Research, Chinese Academy of Sciences, Beijing, China, <sup>2</sup>College of Resources and Environment, University of Chinese Academy of Sciences, Beijing, China, <sup>3</sup>Centre de Recherches Pétrographiques et Géochimiques, UMR7358, CNRS and Université de Lorraine, Vandœuvre-lès-Nancy, France, <sup>4</sup>CAS Center for Excellence in Tibetan Plateau Earth Sciences, Chinese Academy of Sciences, Beijing, China, <sup>5</sup>School of Earth Sciences and Key Laboratory of Western China's Mineral Resources of Gansu Province, Lanzhou University, Lanzhou, China, <sup>6</sup>College of Resources and Environment, Linyi University, Linyi, China

**Abstract** The uplift of the Tibetan Plateau (TP) during the late Cenozoic is thought to be one of crucial factors controlling Asian climate. However, the complex interaction between tectonics and climate change is still unclear. Here we present the first record of clay mineralogy and elemental geochemistry covering ~12.7–4.8 Ma in a fluvial-lacustrine sequence in the Xining Basin. Geochemical provenance proxies (Th/Sc, Zr/Sc, and Cr/Zr) in the <2- $\mu$ m fraction show a significant provenance change at ~8.8 Ma. Silicate-based weathering indexes (CIA, CIW, and PIA) displayed coeval changes with provenance but discrepant changes with regional climate. Since the clay mineralogy exhibits significant change at ~7.8 Ma uncorrelated with modifications in provenance, it can be employed to reveal regional climate change. The rise in illite and associated decrease in the sum of smectite and illite/smectite mixed layers reflect gradual and slow aridification since ~12.7 Ma with intensified drying since ~7.8 Ma until approaching the modern climate status. Our results, together with other regional climatic and tectonic records, clearly illustrate that accelerated uplift of the northeastern TP since ~8–9 Ma has mainly modulated the regional erosion, weathering, transportation, and sedimentation and amplified the global cooling and drying trend toward the regional climate of modern conditions. Our study suggests that in the tectonically active northeastern TP, a comprehensive mineralogical and geochemical investigation of the fine-grained fraction of the basin sediments could retrieve the interactions between tectonics and climate behind the complex change in exhumed lithology and sedimentary routing systems.

## 1. Introduction

The paleoenvironment and paleoclimate of Asia dramatically changed during the late Cenozoic, such as enhanced central Asian aridification (Caves et al., 2016; Ding et al., 2005; Guo et al., 2002; X. D. Liu et al., 2015; Lu & Guo, 2014; Ruddiman & Kutzbach, 1989) and East Asian monsoon development (An et al., 2001; Guo et al., 2002). Generally, uplift of the Tibetan Plateau (TP) could lead to those transitions of paleoenvironmental and paleoclimatic patterns in Asia by blocking moisture from the ocean, reorganizing Asian atmospheric circulation, and strengthening the heating difference between land and ocean (Kutzbach et al., 1989; Li & Fang, 1999; X. D. Liu & Yin, 2002; Manabe & Terpstra, 1974; Tada et al., 2016). Therefore, the uplift of the TP in the late Cenozoic is considered one of the major drivers forcing the Asian paleoenvironmental changes, as evidenced from paleoreconstructions (An et al., 2001; Li et al., 2014; Ma et al., 1998; Xiao et al., 2012; Y. B. Yang et al., 2016) and modeling work (Kutzbach et al., 1989; X. D. Liu & Yin, 2002; X. D. Liu et al., 2015; R. Zhang, Jiang, et al., 2015). However, the complex interaction between tectonic and climate change is still unclear. This is largely due to (1) the combined effect of aridification of the continent by oceanic closure and uplift of the plateau and (2) the lack of temporally and spatially matching tectonic and climatic records in a critical zone. The northeastern TP and its adjacent

central Asia are thought to be ideal regions for revealing the interaction between tectonic uplift and climate because their sediments contain abundant information of tectonics and climate change since the Miocene (e.g., Harris, 2006; Li et al., 2014; Molnar, 2005; Y. B. Yang et al., 2016, and references therein).

A series of sedimentary basins located in the northeastern TP with thick late Cenozoic sediments can provide continuously long archives to reveal the regional topographic and climatic evolution. Numerous studies have shown that widespread uplift started at approximately 8–9 Ma across the northeastern TP, as evidenced by thermochronology methods (Z. L. Chen et al., 2002; Lease et al., 2007; Zheng et al., 2003, 2006, 2010) and sedimentation rates (Fang et al., 2007, 2016; Huang et al., 2006; Li et al., 2014; R. S. Yang, Fang, et al., 2017). This series of contemporaneous uplift events should be attributed to the late tectogenesis of India-Asia collision (Tapponnier et al., 2001). Meanwhile, a nearly concurrent enhancement of aridification also occurred in the central Asian interior and manifested as intensified arid conditions and decreased precipitation amount (Guo et al., 2002; Miao et al., 2012, and references therein). The onset of eolian red clay (fine-grained loess with reddish color) accumulation in the Chinese Loess Plateau (CLP; An et al., 2001; Ding et al., 2001; Qiang et al., 2001) and a notable increase in eolian input to the fluvial basin system on the northeastern TP (Y. B. Yang, Galy, et al., 2017), the sea of Japan (Shen et al., 2017), and the North Pacific (Rea et al., 1998; W. F. Zhang, Chen, et al., 2016) have all been interpreted as evidences of central Asian aridification; yet a new hypothesis interpreted them as a result of more dust supply caused by increased erosion in the Qilian Mountains and low-elevation eastern Asia areas (Nie et al., 2018). Intensified arid conditions and decreased precipitation amount in the northeastern TP and its adjacent regions was also recorded by the replacement of forest by steppe (Hui et al., 2011; J. Liu, Li, et al., 2016; Ma et al., 1998, 2005), abrupt shift of geochemical proxies (Wan et al., 2010; Y. B. Yang et al., 2016), and sharp increase of illite/smectite ratio (Shen et al., 2017). However, the existing tectonic and climatic evidence is temporally simultaneous (~8–9 Ma) but spatially separated in different regions, and thus factors of local sedimentary environment and climatic conditions may bias those records, leading to poor constraints on the exact links between tectonic and climatic forcing mechanisms and processes. Furthermore, in this tectonically active region, other factors, such as changes in landform, bedrock lithology, hydrographic patterns, and sedimentary sorting, may overwhelm the paleoenvironmental significance of proxy records (e.g., Fang et al., 2016). For example, when dealing with a long-term sedimentary sequence, its complex and often poorly known bedrock lithology and frequently evolving sediment routing conditions from source to sink can profoundly bias many widely used whole-rock paleoenvironmental proxies. Clay minerals and their assemblages are potential proxies to reconstruct paleoenvironment in such complex sedimentary routing systems (Singer, 1984; Thiry, 2000; Ye et al., 2018).

To date, the long-term clay mineral records that are needed to reveal the tectonic-climate linkage during the late Cenozoic are lacking in the northeastern TP. Recently, a newly discovered fluvial-lacustrine sedimentary sequence in the Xining Basin, located in the northeastern TP, was precisely dated by magnetostratigraphy and fossil mammals and has an age range from ~12.7 to 4.8 Ma (R. S. Yang, Fang, et al., 2017). Here we present the first clay mineral and geochemical records of the clay fraction (<2  $\mu\text{m}$ ) to better characterize the interplay of the regional climate and tectonic uplift changes.

## 2. Geographic and Geological Settings

The Xining Basin is situated on the northeastern edge of the TP and is a western subbasin of the larger Paleocene-Miocene basin complex named the Longzhong Basin. The basin ranges in elevation between 2,000 and 3,000 m with surrounding mountains reaching approximately 3,700–4,000 m (Horton et al., 2004). The basin is confined by the Riyueshan Mountains, the Dabanshan Mountains, and the Lajishan Mountains to the west, north, and south, respectively, while it is open to the east to the Lanzhou Basin (Figure 1; Dai et al., 2006). Climatically, the basin is located in the transitional zone of the East Asian monsoonal humid region and the central Asian arid region and is thus dominated by a semiarid continental climate (Figure 1a; Xiao et al., 2012). Currently, the annual temperature and precipitation are approximately 6 °C and 415 mm, respectively, with more than 70% of the precipitation falling in June to September derived from the East Asian summer monsoon (Xiao et al., 2012). Because of the large difference in altitude between the low valleys and high mountains of the basin, the modern natural vegetation shows obvious altitudinal gradation, from herbs, coniferous forests, and shrubs to alpine meadows in the upward direction (Chi et al., 2013).

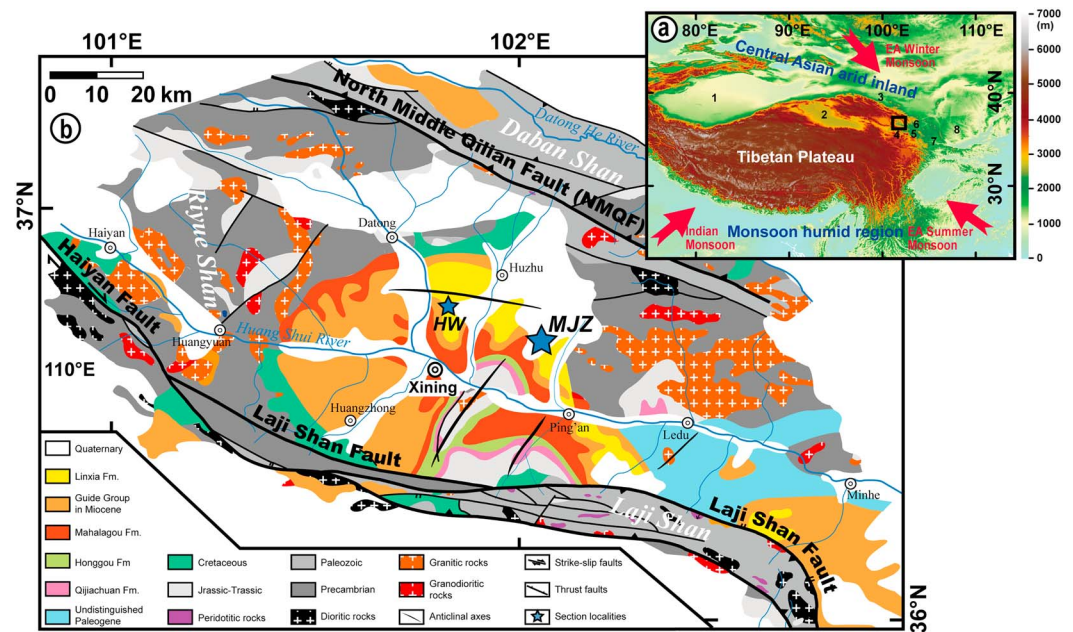


**Figure 1.** (a) Digital elevation model map showing the location of the Xining Basin in the climatic transition region between the arid Asian interior and the East Asian monsoon region. (b) Simplified geologic map of the Xining Basin showing major units and structures and the location of the studied section (modified from Dai et al., 2006). MJZ = Mojiashuang section; HW = Houwan section; EA = East Asian; 1 = Tarim Basin; 2 = Qaidam Basin; 3 = Jiuquan Basin; 4 = Guide Basin; 5 = Linxia Basin; 6 = Lanzhou Basin; 7 = Tianshui Basin; 8 = Chinese Loess Plateau.

The Xining Basin is bounded by two sinistral transpressional faults (the North Middle Qilian Fault to the north and the Laji Shan Fault to the south) and a dextral transpressional Haiyan Fault to the west (Figure 1; Dai et al., 2006). The Cenozoic stratigraphy of the Xining Basin unconformably overlies the Cretaceous alluvial sedimentary rocks or older basement rocks (Horton et al., 2004). With a thickness of more than 1,100 m, the Cenozoic successions are well developed and dominated by fluvio-lacustrine sediments and are divided into the Paleogene Xining Group and Neogene Guide Group according to previous paleontological and lithostratigraphic studies (Qinghai Bureau of Geology and Mineral Resources (QBGMR), 1991; Dai et al., 2006). The Paleogene Xining Group is characterized by distinct siltstone-mudstones and intercalated thick gypsum beds and is further subdivided into the Qijiachuan, Honggou, and Mahalagou Formations in upward sequence based on the presence of gypsum beds and microfossils. The Neogene Guide Group is characterized by an upward coarser grain size and an upward lighter color and contains a limited amount of gypsum. According to the content of sandstones and conglomerates and fossil mammals and microfossils with special age significance, the Guide Group is further subdivided into the Xiejia, Chetougou, Guanjiashan, and Mojiashuang (MJZ) Formations upward (Dai et al., 2006; W. L. Zhang et al., 2017). Detailed paleomagnetic investigations in the Xining Basin show that the Cenozoic stratigraphy of the Xining Basin spans from circa 54 to 4.8 Ma, supported by the biostratigraphic age (Dai et al., 2006; Dupont-Nivet et al., 2007; Horton et al., 2004; Xiao et al., 2012; R. S. Yang, Fang, et al., 2017; Zan et al., 2015).

The position of the Xining Basin in the transitional zone between the arid Asian interior and the humid East Asian monsoon region makes its sedimentary sequence a key archive to study Asian paleoclimatic changes. Previous studies have successfully reconstructed paleoclimatic history from the Eocene to the middle Miocene, such as the late Oligocene Warming, the Middle Miocene Climatic Optimum, and Eocene-Oligocene transition event (Bosboom, Abels, et al., 2014; Chi et al., 2013; Dupont-Nivet et al., 2007; Zan et al., 2015; C. X. Zhang & Guo, 2014).

The studied MJZ section (36°41'07.08"N, 102°04'15.78"E to 36°41'06.95"N, 102°03'04.47"E) is situated in the central east Xining Basin, approximately 25 km northeast of Xining City. The 336-m-thick sequence is characterized by mudstones and siltstones with thin paleosol complexes and marls (0–137 m), coarsening



upward to thick mudstones and siltstones interbedded with thin conglomerates and sandstones (137–252 m) and imbricated boulder conglomerates intercalated with thin siltstones (252–324 m), demonstrating that this sequence underwent stepwise changes in the depositional environments from floodplain via braided river to alluvial (Figure 2; R. S. Yang, Fang, et al., 2017). A suspected eolian deposition (pelitic siltstone with low density) forms the upper part of the section (324–336 m), and a thin loess unit unconformably overlies the MJZ section (Figure 2). The lower part of the section contains abundant late Miocene fossil mammals (Han et al., 2015; R. S. Yang, Fang, et al., 2017), for example, *Parelasmotherium* sp., *Hipparion dongxiangense*, and *Chilotherium wimani*, and together with a high-resolution paleomagnetic study, the MJZ section was deposited from approximately 12.7 to 4.8 Ma (R. S. Yang, Fang, et al., 2017).

### 3. Materials and Methods

Clay minerals are usually the products of chemical weathering of rocks and have a straightforward relationship with climate and environment, with the assumption that duration for chemical weathering is constant (Singer, 1980, 1984; Thiry, 2000). Clay mineral assemblages are potentially more useful proxies for tracing late Cenozoic regional paleoenvironmental changes on the northeastern TP for the following reasons. First, sorting during transportation and deposition is greatly reduced, as clay minerals are extracted from a narrow range of grain size fractions (e.g.,  $<2$  or  $<5$   $\mu\text{m}$ ; Chamley, 1989), and the reported clay mineral contents are normalized to the total portion of clay minerals. Second, clay minerals are the products of catchment weathering that are mainly controlled by regional climate change and basement rock type (Chamley, 1989). However, the main parent minerals of clay formations (e.g., feldspar and mica minerals) are widespread in various lithologies of the upper continental crust (Taylor & McLennan, 1985). Clay mineral distributions of modern global continental soils and Chinese soils exhibit a first-order climatic control rather than a lithology change (Chamley, 1989; Y. Xiong, 1986). Meanwhile, the obvious clay mineral differentiations in large rivers (e.g., Yellow and Yangtze rivers) follow a distinct climatic gradient regardless of regional lithology (Pang et al., 2018; Shen et al., 2017). Therefore, the clay mineral assemblages are less sensitive to provenance change than other proxies. Furthermore, previous studies have also shown that clay minerals in most fresh/saline water are almost exclusively eroded from the drainage area with negligible contribution from their formation in the water column or at the sediment-water interface (Chamley, 1989). In addition, diagenetic clay minerals can be easily distinguished by several classical methods (Dunoyer de Segonzac, 1970; Hillier, 1995; Hong et al., 2007; Huyghe et al., 2011; Ye et al., 2018) and are always less important in continental drainage basins (Chamley, 1989; Gao, 2017). Overall, clay mineral assemblage is one of the most reliable proxies for reconstructing paleoenvironmental changes in stratigraphy with complex lithology and changing facies over different timescales, especially for the longer timescales in continental fluvial basins (Gylesjö & Arnold, 2006; Hong et al., 2010, 2017; Singer, 1980; Song et al., 2018; Wang et al., 2011, 2013; C. X. Zhang & Guo, 2014; C. X. Zhang, Xiao, et al., 2015) and ocean/marginal sea basins (Z. F. Liu et al., 2003, 2010; Z. F. Liu, Zhao, et al., 2016; Shen et al., 2017; Singer, 1984; Thiry, 2000).

X-ray diffraction (XRD) has been performed on six mudstone-siltstone bulk samples spanning the entire section at large interval ( $\sim 30$ – $50$  m) and on four eolian sediment samples from the Xining Basin (Figure 3). For  $<2$ - $\mu\text{m}$  clay fractions analysis, 118 samples were chosen at 2.5-m stratigraphic intervals, wherever possible, along the 336-m-thick MJZ section. However, the interval was lengthened to  $\sim 5$ – $10$  m for sampling only lenses of mudstones, siltstones, or sandstones where the lithology was dominated by conglomerates. Besides, six samples from MJZ modern loess and six samples of red clay from the Houwan (HW) section were selected for clay mineral analysis. Age constraint of samples from the HW section was based on the chronology reported in W. L. Zhang et al. (2017).

Separation of the separating clay fractions from bulk samples used  $\sim 30$  g placed into a 1-L beaker. Twenty-five percent  $\text{H}_2\text{O}_2$  and 1-M acetic acid in a water bath at  $50^\circ\text{C}$  was added for 12 hr with occasional oscillation to remove organic matter and carbonate, respectively. After removing residual acetic acid and free ions using ultrapure water ( $18.2$  M $\Omega$ -cm at  $25^\circ\text{C}$ ), the clay fractions were separated by gravitational sedimentation following Stokes' law (Zeng et al., 2010). In brief, after being well stirred, the samples were kept at room temperature ( $\sim 20^\circ\text{C}$ ) for 8 hr and then the suspension liquid of the upper 10 cm was siphoned away. Finally, the  $<2$ - $\mu\text{m}$  clay fractions were separated by centrifugation.

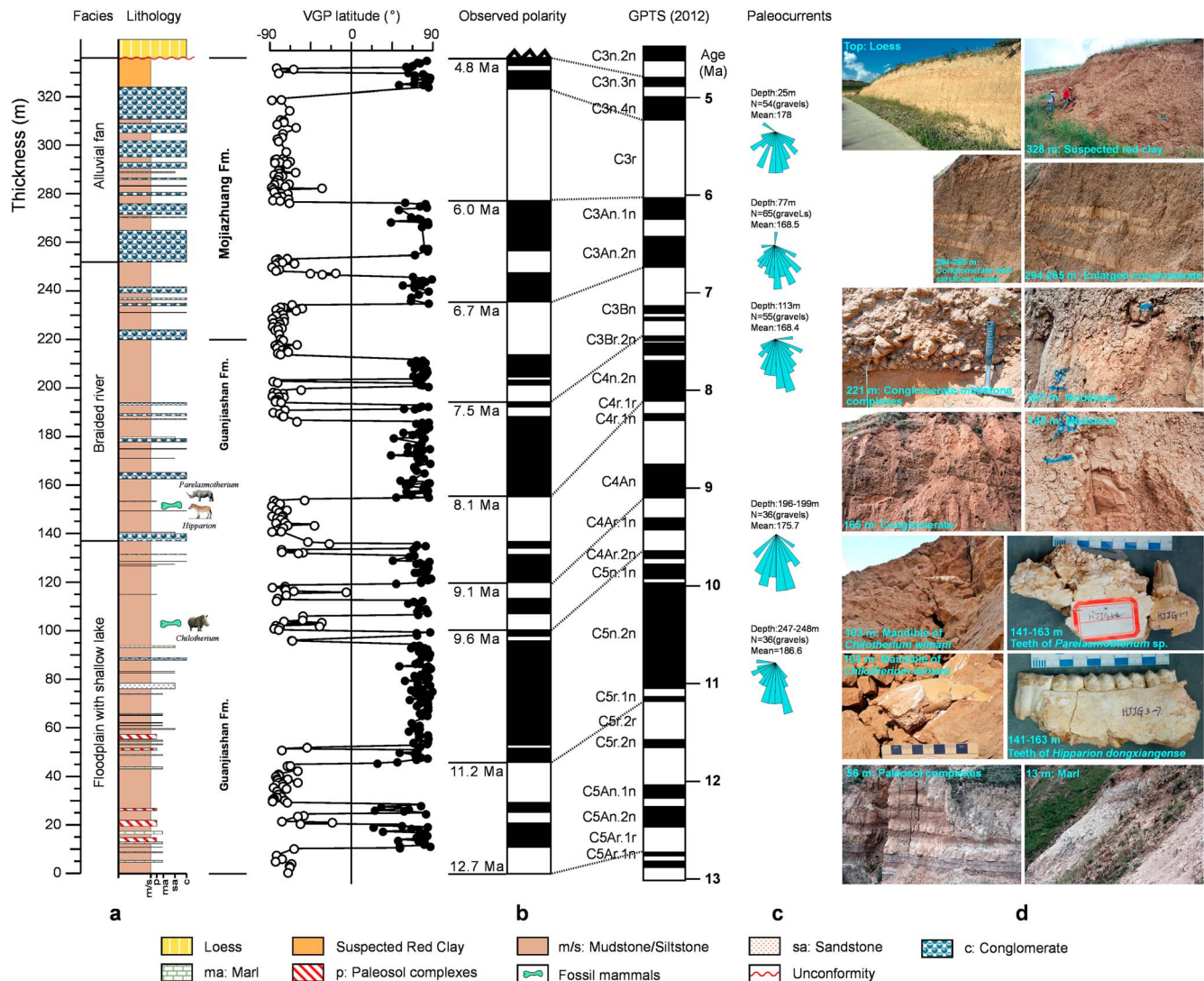


**Figure 2.** Sedimentology of the Mojiazhuang section. (a) Lithology and sedimentary facies; (b) virtual geomagnetic pole (VGP) latitude, magnetostratigraphy, and its correlation with the geomagnetic polarity time scale (GPTS; Ogg et al., 2012); (c) dominant paleocurrent (all predominantly from the S); and (d) representative photos (R. S. Yang, Fang, et al., 2017).

To identify and quantify the clay minerals, each sample was suspended and deposited onto glass slides and allowed to air-dry at room temperature. After XRD analysis carried out on air-dried (AD) samples, they were treated with ethylene glycol vapor for 24 hr and heated at 450 °C for 2 hr after ethylene glycol solvation. Thus, each sample includes the AD, ethylene glycol-saturated (EG), and heated XRD patterns. XRD patterns were measured using a Rigaku D/MAX-2000 diffractometer (Cu,  $K\alpha$ , 1.5406 Å, 40 kV, 100 mA, 3–30°, step 0.02°, 10°/min) at the Micro Structure Analytical Laboratory, Peking University.

Identification of clay minerals from the three XRD patterns was performed in JADE 6.5 software and was primarily based on the position of the (001) series of basal reflections as described by Moore and Reynolds (1997). Kaolinite and chlorite have almost coincident peaks of a characteristic peak (7.1 Å) on EG diffractogram (Figure 4). The distinction between kaolinite and chlorite is mainly based on the (002) peak (3.58 Å) of kaolinite and the (004) peak (3.54 Å) of chlorite (Figures 4a and 4d). In addition, chlorite was also recognized based on its characteristic (001) peak (14.2 Å) and (003) peak (4.74 Å) on the EG diffractogram. Illite is usually recognized by peaks at 10 (001), 5 (002), and 3.33 Å (003), and those peaks display no changes on EG diffractogram (Figure 4).

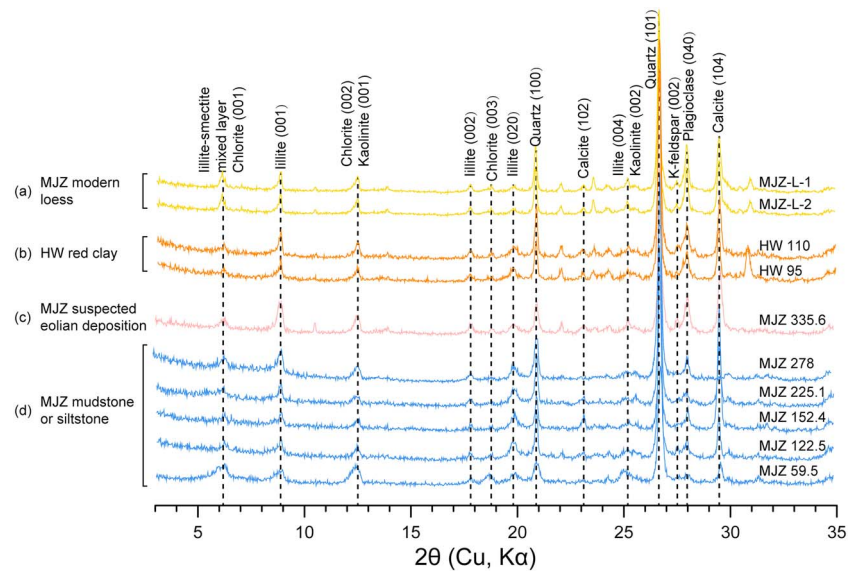


**Figure 3.** X-ray diffraction analyses of 10 bulk samples. (a) Top modern loess from the MJZ section; (b) red clay from the HW section; (c) suspected eolian deposition from the top of the MJZ section; and (d) mudstone or siltstone from the MJZ section. Numbers in the sample's name correspond to the stratigraphic height in meter, starting from the bottom. MJZ = Mojia Zhuang; HW = Houwan.

According to the content of smectite in illite/smectite (I/S) mixed layers, I/S mixed layers can be divided into regular I/S mixed layers (<50%) and irregular I/S mixed layers (>50%; Reynolds, 1980). I/S mixed layers and smectite are typical expandable clay minerals that exhibit similar wide peaks at approximately 12–15 Å on an AD diffractogram. The distinctions among smectite, irregular I/S mixed layers, and regular I/S mixed layers

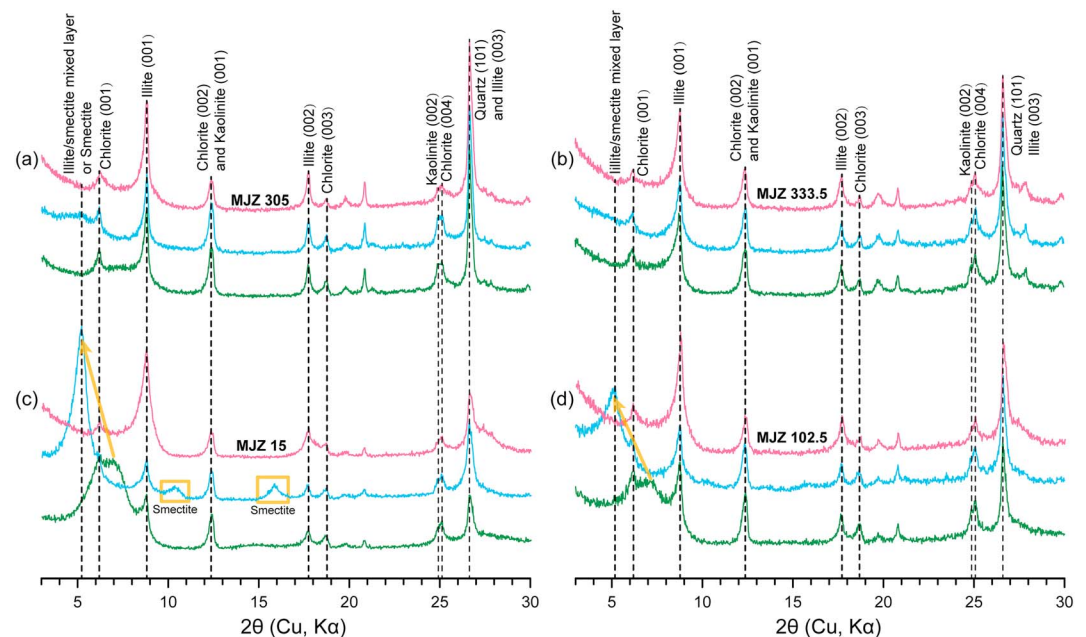


**Figure 4.** X-ray diffraction patterns of four representative samples of clay fractions. Samples of (a) typical (002) peak of kaolinite and (004) peak of chlorite; (b) regular illite/smectite mixed layers; (c) high content of smectite; and (d) irregular illite/smectite mixed layers. Green, blue, and red lines represent the air-dried, ethylene glycol-saturated, and heated X-ray diffraction patterns, respectively. Arrows show the peak shifts of smectite (c) and illite/smectite mixed layers from the air-dried sample to the ethylene glycol-saturated samples.



can be recognized by a combination of the AD and EG diffractograms. After being treated with ethylene glycol, the 12- to 15-Å peak of smectite will be transferred to 17 Å, and a series of new peaks will appear at 8.5, 5.67, and 4.25 Å (Figure 4c). The 12- to 15-Å peak of the irregular I/S mixed layers on an AD diffractogram will be transferred to 17 Å, but no peaks will appear on an EG diffractogram at 8.5, 5.67, and 4.25 Å (Figure 4d), while the 12- to 15-Å peak of the regular I/S mixed layers will not be transferred to 17 Å on an EG diffractogram (Figure 4b).

After the identification of each clay mineral, semiquantitative estimates were based on peak areas of the basal reflections following “SYT 5163-2010” (Zeng et al., 2010), which is an improved method of Schultz (1964). The content of illite is calculated by the area of the 10-Å peak, while the total contents of kaolinite and chlorite are calculated by the area of the 7.1-Å peak. The relative proportions of kaolinite and chlorite are calculated based on the areas of the 3.58-Å peak for kaolinite and the 3.54-Å peak for chlorite (Biscaye, 1965). The remnant part should be smectite and I/S mixed layers, and the relative content of smectite is calculated by the peak area of the 17-Å peak. The proportion of smectite layers in the I/S mixed layers was estimated based on a method derived from Reynolds (1980), and a detailed description can be found in Ye et al. (2016).

Major and trace elements of the <2-μm clay fractions of the MJZ section were measured by an inductively coupled plasma optical emission spectrometer (Leeman Labs Prodigy-H) and an inductively coupled plasma mass spectrometer (X-7; Thermo-Elemental, USA), respectively, at the Institute of Tibetan Plateau Research, Chinese Academy of Sciences, Beijing. For this, the oven-dried clay fractions were ground into powder and digested by pressurized acid digestion using a mixture of nitric acid and hydrofluoric acid (Y. B. Yang et al., 2015). Relative standard deviations from the mean value of replicate analyses were less than 5%.

## 4. Results

### 4.1. Clay Minerals

The XRD analyses of bulk rocks show that the sediments of the MJZ section have mineral compositions that are mostly similar to local red clay and modern loess (Figure 3), even though they were collected from different facies and lithological layers. The mineral assemblage mainly contains quartz, plagioclase, K-feldspar, calcite, and clay minerals.

The clay mineral results of the <2-μm fractions show that the major components are I/S mixed layers, illite, chlorite, and kaolinite, with limited amount of smectite (Figure 4). In this study, we group the I/S mixed layers and smectite as “total smectite” since I/S mixed layers are often the product of the diagenetic transformation of smectite to illite in old sequences (Chamley, 1989). Total smectite and illite are the dominant clay minerals and correspond to over 75% in each sample, while chlorite and kaolinite are present as minor components. More specifically, the range and average (in bracket) are as follows: total smectite 22–76% (50.8%), illite 16–56% (34.6%), chlorite 0–21% (8.2%), and kaolinite 0–15% (6.4%). Illite and chlorite exhibit upward increase. Total smectite and kaolinite display an upward declining trend along the studied section (Figure 5). In more detail, total smectite shows a slightly decreasing trend at 12.8–7.8 Ma and a more pronounced decrease since 7.8 Ma, while illite exhibits nearly the opposite trend. Chlorite shows a slight rise with time, while kaolinite performs a general decrease since 12.7 Ma but an obvious increase at 6.3–4.8 Ma. The total smectite was well inversely correlated with illite (Figure 6). Interestingly, kaolinite and chlorite exhibit a significantly negative relationship before 7.8 Ma but have no correlation at 7.8–4.8 Ma (Figure 6). It is worth noticing a lack of rise in the illite content of the I/S mixed layers with depth (Figure 5).

### 4.2. Major Elements

The intensity of chemical weathering has been estimated by several proxies in the literature such as the chemical index of alteration ( $CIA = [Al_2O_3 / (Al_2O_3 + CaO + Na_2O + K_2O)] \times 100$ ; Nesbitt & Young, 1982), the chemical index of weathering ( $CIW = [Al_2O_3 / (Al_2O_3 + CaO + Na_2O)] \times 100$ ; Harnois, 1988), and the plagioclase index of alteration ( $PIA = [(Al_2O_3 - K_2O) / (Al_2O_3 + CaO + Na_2O - K_2O)] \times 100$ ; Fedo et al., 1995) using the molar percentage of oxides in the silicate fraction. In this study, we calculated these three indexes based on the carbonate-free clay fractions of our samples. In addition, the ratios of Ca/Al, Na/Al, and K/Al are also considered useful proxies to trace chemical weathering due to the



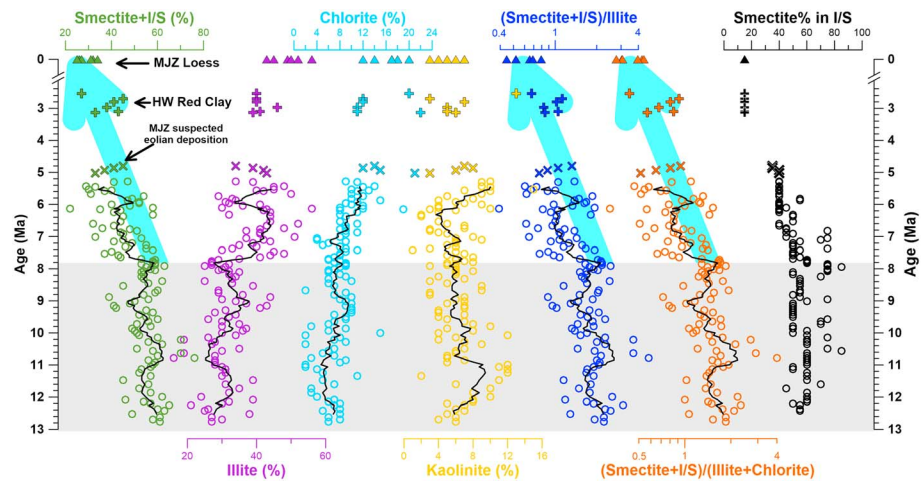


**Figure 5.** Relative abundances of clay mineral assemblages and ratios from the MJZ and HW sections. The age assignments of measured samples are interpolated based on magnetostratigraphy (R. S. Yang, Fang, et al., 2017; W. L. Zhang et al., 2017). The bold black line displays the seven-point running average for the MJZ section sediments (the data of the top eolian deposits are not included in the running average). The bold blue arrows show the consistent evolutions of clay minerals and their ratios in the post-7.8 Ma MJZ section sediments and local eolian deposits from 7.8 Ma to present. I/S = illite/smectite mixed layers; MJZ = Mojiashuang; HW = Houwan.

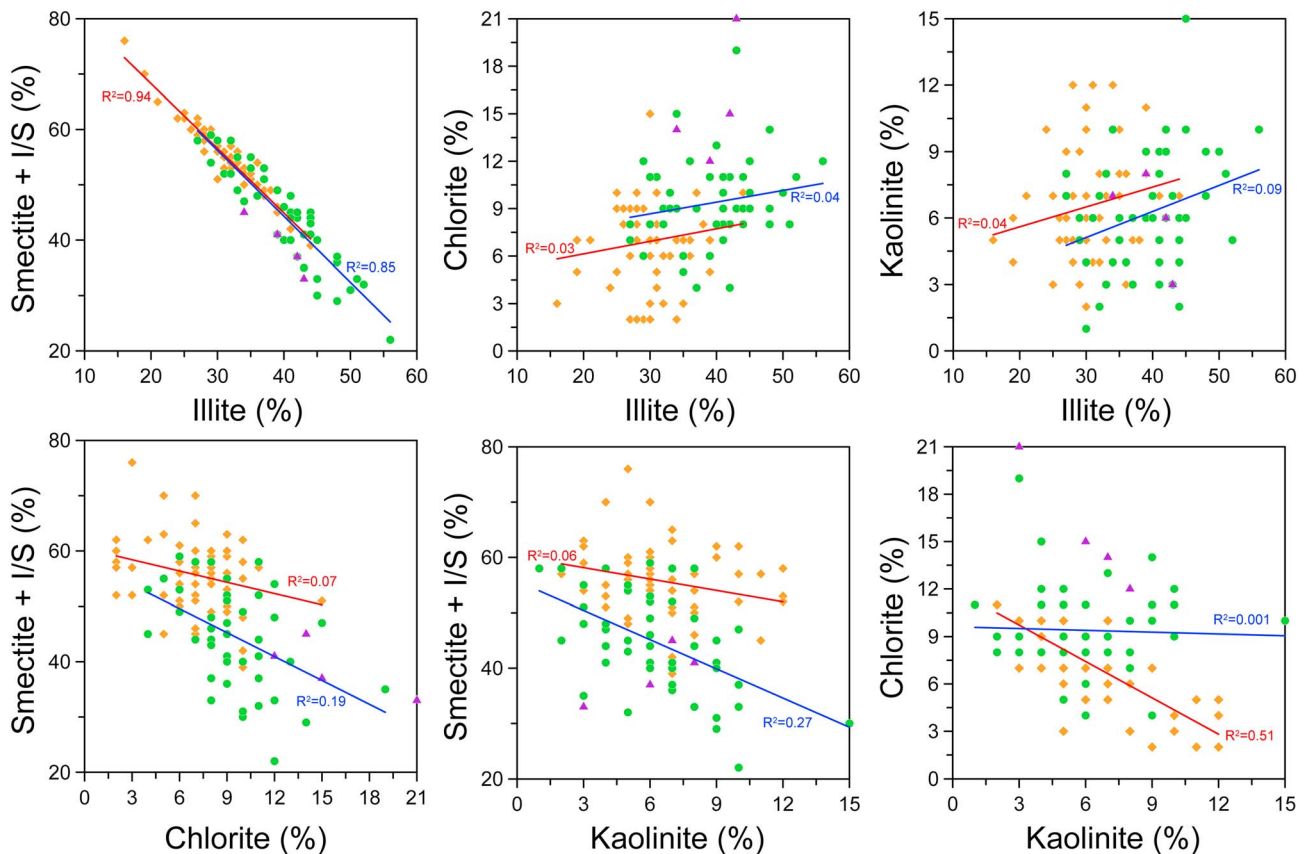


**Figure 6.** Correlations between different clay minerals in the Mojiashuang section sediments. Orange, green, and purple symbols represent samples before 7.8 Ma, after 7.8 Ma, and top eolian deposits, respectively. Red and blue fitting lines are related to samples before 7.8 Ma and after 7.8 Ma, respectively. I/S = illite/smectite mixed layers.

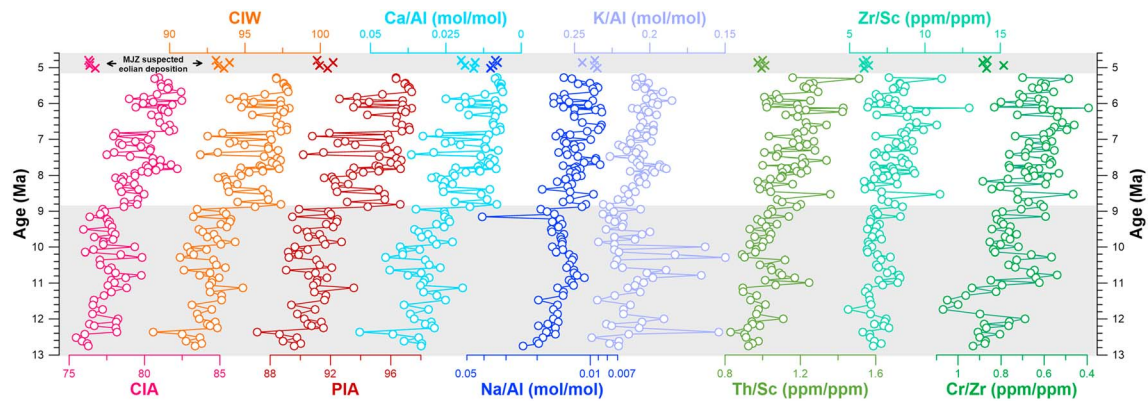


**Figure 7.** Depth profiles of various weathering and provenance proxies in the  $<2\text{-}\mu\text{m}$  fraction of the MJZ section sediments. Note the significant changes in all proxies at  $\sim 8.8$  Ma and the sharp difference between the clay and the eolian deposits in the MJZ section sediments. MJZ = Mojiazhuang

distinct mobility of Ca, Na, K, and Al in the critical zone. The results show that CIA, CIW, and PIA exhibit similar upward evolutions characterized by an abrupt increase at  $\sim 8.8$  Ma from the generally lower values in the lower section to high values in the upper section (Figure 7). Ca/Al, Na/Al, and K/Al of carbonate-free clay fractions generally exhibit upward decreasing trends in contrast to those of the above three weathering indexes (Figure 7). As shown in Figure 8, the CIA has a generally positive correlation with Ca/Al, Na/Al, and K/Al ratios, while the CIW and PIA have positive correlations with the Ca/Al and Na/Al ratios and poor correlations with the K/Al ratio.

#### 4.3. Trace Elements

Trace elements and their ratios are also widely used in the provenance characterization of various sediments (McLennan et al., 1993; Taylor & McLennan, 1985). Along this section, we found an abrupt rise at  $\sim 8.8$  Ma of the Th/Sc, Zr/Sc, and Cr/Zr ratios superimposed on an upward increase throughout the section (Figure 7). The CIA, CIW, and PIA in the MJZ section show similar temporal trends with Th/Sc, Zr/Sc, and Cr/Zr resulting in significant correlation coefficients between these parameters (Figure 9). The La-Th-Sc ternary diagram shows relatively restricted distributions of top eolian deposits, the post-8.8 Ma, and pre-8.8 Ma samples in the MJZ section (Figure 10c). Our samples exhibit La-Th-Sc distributions that are similar to those in the  $<5\text{-}\mu\text{m}$  fractions of the northern Chinese deserts but a significant La depletion compared with Post-Archaean average Australian Shale (PAAS; McLennan, 1989) and eolian deposition in the CLP (Liang et al., 2009). Top eolian deposits and pre-8.8 Ma samples have similar La-Th-Sc distributions and show relative depletion of La and enrichment of Sc and Th.

## 5. Discussions

### 5.1. Origins of Clay Minerals in the MJZ Section

In general, clay minerals in basin sediments can be generated by erosion and weathering of fresh bedrocks and soils, produced in situ in river and lake water, and formed by diagenetic modifications shortly after deposition and during burial (Chamley, 1989; Fagel, 2007; Thiry, 2000). In rare cases, clay mineral formation in riverine and lake systems and diagenesis can blur the climate sensitivity of detrital clay minerals in the basin associated with the weathering of bedrocks catchment (Q. Chen et al., 2017; Huyghe et al., 2011; Singer, 1984; Thiry, 2000; Ye et al., 2018), and we will discuss these aspects in detail.

First, burial diagenesis can result in the transformation of detrital clay minerals such as smectite to illite, which may bias the climatic significance of clay mineral assemblages (Chamley, 1989; Ye et al., 2016) since the most widespread diagenetic modification of clay minerals in sedimentary basins is the illitization of smectite (Chamley, 1994). According to the classical diagenesis model by Weaver (1984), when diagenesis plays a major role in regulating illite and smectite contents, the illite proportion in I/S mixed layers and illite content are expected to exhibit gradual increases with rise of temperature and pressure caused by the rise of the burial depth. Two main potential mechanisms were proposed to explain this transition: (1) smectite layers are converted into I/S mixed layers and/or illite layers using  $\text{Al}^{3+}$  and  $\text{K}^+$  released on the

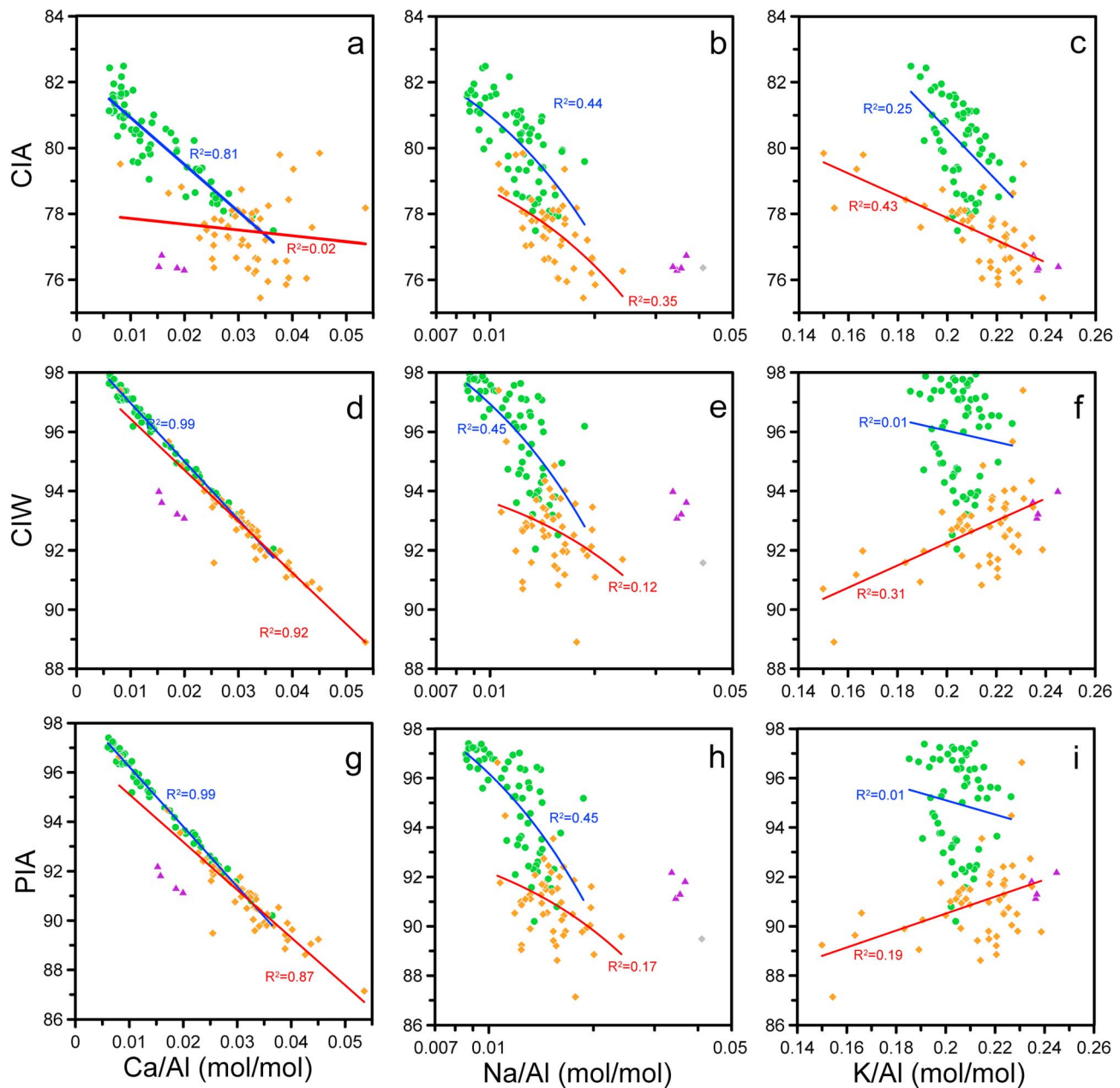


**Figure 8.** Relationships between classic silicate weathering proxies (CIA [a–c], CIW [d–f], and PIA [g–i]) versus oxide ratios (e.g., Ca/Al, Na/Al, and K/Al). Orange, green, and purple symbols represent samples before 8.8 Ma, after 8.8 Ma, and top eolian deposits, respectively. Red and blue fitting lines are based on samples before 8.8 Ma and after 8.8 Ma, respectively. CIA = chemical index of alteration; CIW = chemical index of weathering; PIA = plagioclase index of alteration.

decomposition of K-feldspar and mica (Ahn & Peacor, 1986; Hower et al., 1976); (2) the illitization of smectite results from two paralleled processes of solution of smectite and recrystallization of illite (Nadeau et al., 1984). Our results show an opposite trend compared with the classical depth profile of clay mineral diagenesis. Specifically, a downward decrease in illite content and relatively stable illite proportion in the I/S mixed layers (Figure 5) indicates very little diagenetic change that occurred during and after deposition of the studied MJZ section sediments. This may be mostly due to the fact that the burial depth of the studied section is limited to only 336 m, while the diagenetic transformation of smectite to illite always occurs within a burial depth of more than 1,500 m (Chamley, 1989) with pressures and temperatures over 900–920 kg/cm<sup>2</sup> and 100–140 °C, respectively (Aoyagi & Kazama, 1980).

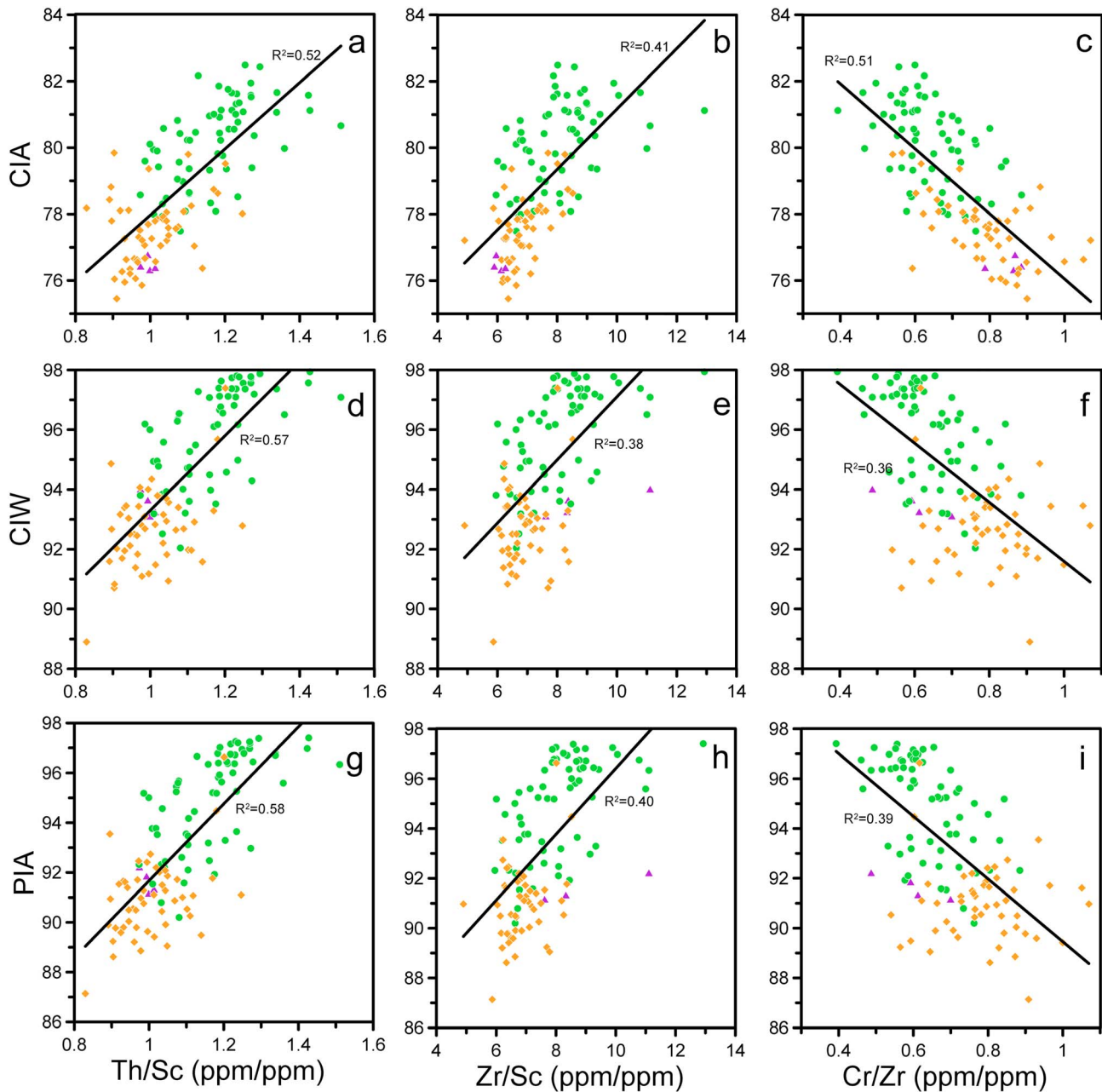


**Figure 9.** Relationships between classic silicate weathering proxies (CIA [a–c], CIW [f–h], and PIA [g–i]) versus provenance proxies (Th/Sc, Zr/Sc, and Cr/Zr). Orange, green, and purple symbols represent samples before 8.8 Ma, after 8.8 Ma, and top eolian deposits, respectively. Correlation analysis is always based on all samples, and in all cases  $P$  values are less than 0.001. CIA = chemical index of alteration; CIW = chemical index of weathering; PIA = plagioclase index of alteration.

Second, regarding authigenic clay minerals formed from the paleowater body, previous investigations of clay mineral origins of modern worldwide terrigenous basins have indicated that fluvial and lacustrine clay minerals have predominant detrital characteristics similar to their surrounding drainage basins (Chamley, 1989; Court et al., 1972; McMurtry & Fan, 1974; Tomadin et al., 1986). A lack of sufficient prerequisite cations in rivers and freshwater lakes and silicon in saline lakes may be the reason why authigenic clay minerals are scarce in most fresh and saline water (Gao, 2017). Therefore, we reasonably assume that there are minor authigenic clay minerals in the fluviolacustrine sediments of the MJZ section. In addition, the amount of insoluble trace element such as La or Th (supporting information table) in the clay fraction is



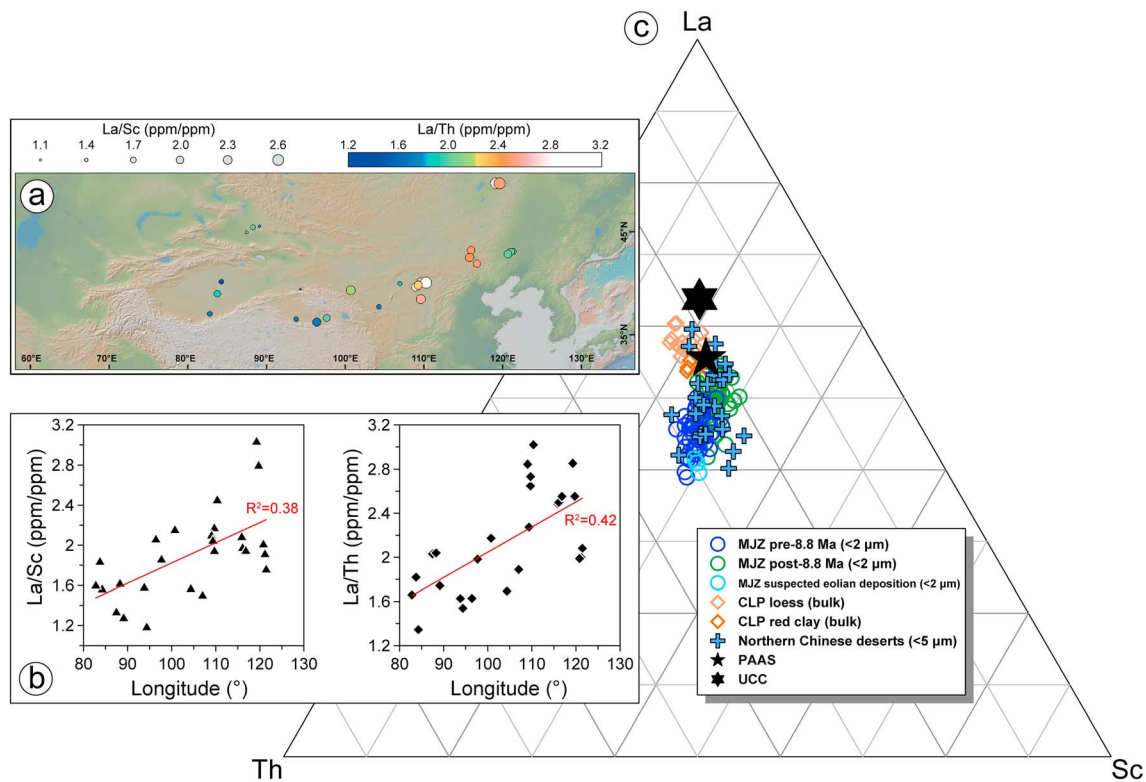


**Figure 10.** Comparison of the Sc, La, and Th abundances between the clay fraction of the MJZ section (this study) and the <5- $\mu\text{m}$  Chinese northern desert sand (data available from W. F. Zhang, Chen, et al., 2016). (a) Digital elevation model map showing La/Th and Th/Sc ratios of <5- $\mu\text{m}$  Chinese northern desert sand; (b) relationship between La/Th and Th/Sc ratios and longitudes of Chinese northern deserts; (c) La-Th-Sc ternary diagram of top eolian deposits, post-8.8 Ma, and pre-8.8 Ma samples in the MJZ section; bulk loess and red clay in the Xifeng section (Liang et al., 2009); and <5- $\mu\text{m}$  fractions of Chinese northern desert sand, upper continental crust (UCC, Taylor & McLennan, 1985) and Post-Archaean average Australian Shale (PAAS; McLennan, 1989). MJZ = Mojiazhuang.

close to the upper continental crust composition and therefore is not compatible with a significant occurrence of clay minerals directly precipitated in rivers and freshwater lakes. After excluding diagenetic and authigenic influence, most of the clay minerals of the studied MJZ section should be of detrital origin and can be exploited to retrieve the late Miocene catchment changes in the Xining Basin.

## 5.2. Provenance Change in the MJZ Section

Provenance change should be assessed in advance when proxies based on clay mineral and element ratios of the <2- $\mu\text{m}$  fractions are used to reconstruct paleoclimate. The Th/Sc ratio is useful for tracing igneous differentiation because Th is a typically incompatible element in igneous systems, yet Sc is compatible (McLennan et al., 1993). The Zr/Sc ratio is regarded as an index of zircon enrichment since Zr is strongly enriched in zircon but not Sc (McLennan et al., 1993; Taylor & McLennan, 1985). Zircon enrichment since ~8.8 Ma in the MJZ section, as indicated by the increased Zr/Sc ratio, may result from provenance change and/or an increase in grain size (Figures 2 and 7). However, the nearly parallel curves and positive relationship between the Th/Sc and Zr/Sc ratios ( $R^2 = 0.77$ ) of the studied section imply that provenance change is the primary control rather than an increase in grain size (McLennan et al., 1993). The Cr/Zr ratio is also a widely used proxy for provenance change because it is an indicator of the mafic versus felsic rocks (Wronkiewicz & Condie, 1987). Concurrent apparent shifts of the Th/Sc, Zr/Sc, and Cr/Zr ratios jointly indicate a provenance change at ~8.8 Ma during the sedimentation of sediments (Figure 7). Increases in the Th/Sc, Zr/Sc, and Cr/Zr ratios suggest an increase in the felsic and/or a decrease in the mafic provenance contribution since ~8.8 Ma. This interpretation is supported by the modern distribution of rocks around the Xining Basin. According to detailed geologic map of the Xining Basin, much more Paleozoic felsic rocks outcrops in the northwest of the studied section rather than in the southwest (J. Zhang, Wang, et al., 2016). This distribution of felsic rocks around our section matches tectonic uplift of the northern boundary of the

Xining Basin (the Dabanshan Mountains; Figure 1) at ~8.6 Ma (R. S. Yang, Fang, et al., 2017), which may lead to more felsic rocks input and thus the rise of those ratios.

Windblown dust is an important source of fine (clays size) sediment in the semiarid and arid regions and can reflect the average conditions of physical and chemical weathering across a broad Earth surface. There was an obvious increase in dust accumulation in the downwind region at approximately 8–9 Ma due to enhanced central Asian aridification (e.g., An et al., 2001; Rea et al., 1998; Y. B. Yang, Galy, et al., 2017) or enhanced precipitation-driven eolian production (Nie et al., 2018). However, the unit at the top of the MJZ section, which is suspected to be heavily influenced by eolian dust, exhibits quite low Th/Sc and Zr/Sc and high Cr/Zr ratios by comparison with the clay fraction of the MJZ section (Figure 7). Interpreting the differences in Th/Sc, Zr/Sc, and Cr/Zr ratios as differences in provenance, the clay fraction of the MJZ section is poorly influenced by dust deposition. In addition, post-8.8 Ma samples of the MJZ section are within the field constrained by the <5- $\mu\text{m}$  fraction of desert sands in North China in the La-Th-Sc plot (Figure 10; data available from W. F. Zhang, Chen, et al., 2016), allowing to distinguish sediments derived from the silicic and basic source rocks (Cullers, 1994). Moreover, the La/Th and La/Sc ratios in those deserts are generally positively correlated with the longitude (Figure 10; W. F. Zhang, Chen, et al., 2016), suggesting distinct dust source provenance between the northwestern and northeastern deserts or a sorting effect. And the post-8.8 Ma data in the MJZ section sediments are characterized by La/Th and La/Sc ratios that are higher than those in the <5- $\mu\text{m}$  fraction from the deserts in northwest China, which are the potential dust sources for the Xining Basin. However, the deserts and likely the low-elevation areas in northeastern China characterized by higher La/Th and La/Sc ratios than post-8.8 Ma data have been recently regarded as dust sources (Nie et al., 2018) and the data of the MJZ section would, in that case, suggest that the Xining Basin was subjected to the combined effects of northeasterly and westerlies wind transport of dust to the basin. Such combined influence of dust source is not supported by the Th/Sc ratio, significantly higher in the clay fraction of the post-8.8 Ma data of the MJZ section ( $1.17 \pm 0.11$ ) than in the eolian deposits of the upper part of the section ( $1.00 \pm 0.03$ ) or the deserts of low-elevation areas in northeastern China ( $0.88 \pm 0.12$ ). Therefore, the potential provenance change is (1) unlikely to be related to changes in the wind direction with a prevailing westerlies system already dominant for the bottom age of the MJZ section and (2) most likely caused by the uplift of the northeastern TP at approximately 8.8 Ma, which leads to exposure and erosion of more felsic material in the drainage area.

### 5.3. Assessment of Provenance Control on Elemental and Clay Mineral Records

The intensity of chemical weathering is often estimated by the CIA (Nesbitt & Young, 1982), CIW (Harnois, 1988) and PIA (Fedó et al., 1995). The CIA is the most widely used index of chemical weathering that is based on the easy removal of labile elements such as Ca, Na, and K relative to a stable residual element such as Al during weathering processes (Nesbitt & Young, 1982). Because K displays less mobile characteristics compared to Ca and Na during weathering and is also involved in postdepositional change, the CIW and PIA were used to evaluate weathering intensity excluding K (Fedó et al., 1995; Harnois, 1988). Similarly, the Ca/Al, Na/Al, and K/Al ratios can also be used to trace chemical weathering due to the substantial differences in mobility during weathering among Ca, Na, K, and Al (S. F. Xiong et al., 2010). However, these indexes are also prone to be affected by sedimentary sorting during transportation, burial diagenesis, and provenance.

All weathering proxies in the MJZ section show an apparent rise at ~8.8 Ma unlikely to be attributed to “intense chemical weathering” for the following reasons. First, this transition of proxies is inconsistent with the long-term aridification of central Asia during the late Cenozoic (Caves et al., 2016; Ding et al., 2005; Guo et al., 2002; Ruddiman & Kutzbach, 1989), which should lead to reduction in the intensity of chemical weathering. Although a new hypothesis suggests that East Asian summer precipitation increased in the discrete intervals of ~8–7.5 and ~6.5–6 Ma (Nie et al., 2018), it is still obviously discrepant with the weathering proxies in the Xining Basin showing a rather monotonous pattern during the 8.8–5.2 Ma interval (Figure 7). Further, the increase of uplift-driven monsoon-induced precipitation is quite obvious in the typical monsoon region, for example, the central CLP, but shows a complex pattern in marginal monsoon regions especially the mountainous basins on the northern TP (X. D. Liu et al., 2015). Therefore, all the conventional weathering intensity records are likely to be biased by other factors. First, sedimentary sorting may redistribute minerals in different grain size fractions. However, the elemental compositions are restricted within the

<2- $\mu\text{m}$  fraction, and sedimentary sorting seems to have a minor influence. Second, the weak diagenesis as shown by clay mineral assemblages may suggest a limited effect on the major element composition in the <2- $\mu\text{m}$  fraction. Third, the tight correlation between the weathering indexes and the provenance tracers, for example, the Th/Sc, Zr/Sc, and Cr/Zr ratios and their evolutionary patterns, suggests the dominating provenance control of the weathering indexed transitions at 8.8 Ma (Figure 7). This is supported by the observations that the post-8.8 and pre-8.8 Ma data exhibit different distributions between the weathering indexes (CIA, PIA, and CIW) and the elemental ratios (Ca/Al, Na/Al, and K/Al; see different fit lines in Figure 8), except for the plots of CIW versus Ca/Al and PIA versus Ca/Al (Figure 8). Moreover, chlorite and kaolinite both have high CIA, CIW, and PIA values but with opposite environmental implications. The concurrent increases in chlorite and kaolinite contents since  $\sim$ 6.3 Ma possibly suggest another provenance change since then and contribute to the increases in the CIA, CIW, and PIA to some extent (Figures 5 and 6).

Despite the dominance of provenance control on the elemental geochemistry of the <2- $\mu\text{m}$  fraction in the MJZ section, provenance change showed a very limited effect on clay mineral assemblages. Clay minerals and their assemblages have poor correlation with provenance proxies in our section, and obvious changes in the total smectite and illite that occurred at  $\sim$ 7.8 Ma are not consistent with the apparent provenance change at  $\sim$ 8.8 Ma (Figures 5 and 7). In addition, the significant increase in kaolinite at 6.3–4.8 Ma is likely to be related to a modification of the catchment detrital input, but its quite low content will not modify the general evolution of clay mineral assemblages. Moreover, the major clay minerals (total smectite, illite, and chlorite) exhibit fairly uniform distributions (similar fit lines in terms of slope) between pre-7.8 and post-7.8 Ma data (Figure 6), which is quite different from those for the weathering indexes (Figure 8). Therefore, after excluding the effects of authigenesis, diagenesis, and provenance, the clay mineral assemblage in the MJZ section is considered to reflect changes in the weathering conditions at the catchment scale, which may be controlled by climate (controlling reaction rates) and/or the duration for weathering (partly controlled by tectonic via physical erosion).

#### 5.4. Late Miocene Aridification on the Northeastern TP

Chlorite in the clay fraction can be produced by physical weathering and the grinding of metamorphic chlorite or weak chemical weathering in arid and cold environments (Ducloux et al., 1976; Vanderaverroet, 2000). Similarly, illite is usually derived from silicate minerals such as mica minerals under dry and cold climates and weak alkaline conditions (e.g., Wang et al., 2013). Smectite may originate from direct alteration of volcanic materials regardless of climatic condition or by the weathering of illite under drier climate (Chamley, 1989; Hong et al., 2007). I/S mixed layers usually correspond to the incomplete transformation of illite or smectite (Hong et al., 2007). Therefore, the very small amount of pure smectite associated to the large occurrence of I/S mixed layers suggests that the smectite from the MJZ section originated from weathering. And the total smectite that is the combination of smectite and I/S mixed layers can be considered as the product of the intermediate stage of chemical weathering, which often develops in temperate and humid climates (Wang et al., 2011; C. X. Zhang & Guo, 2014). Kaolinite is usually rapidly formed in regions with hot and wet climates, such as red earth, which provide conditions for intense weathering by active hydrolysis and ion leaching (Singer, 1980; Wang et al., 2011; C. X. Zhang & Guo, 2014). Chlorite and illite represent minerals in the early stage of weathering and can be altered into smectite and further transform to kaolinite under warm and humid climate conditions (Chamley, 1989). Apart from the climate, the duration is another factor to influence chemical weathering (e.g., Clift et al., 2014; Nie et al., 2014). Under constant climate conditions, short duration of weathering likely results in clay mineral assemblages of earlier stage than long duration (Thiry, 2000). As a result, chlorite and illite can be considered as characteristic of early weathering, while smectite and kaolinite are products of intermediate and late stages of weathering, respectively. Based on this, clay mineral assemblages, such as (kaolinite+smectite)/(illite+chlorite) and smectite/illite, are excellent indicators for tracing the weathering and climate of a source area (e.g., Bouquillon et al., 1990; Kemp et al., 2016; Z. F. Liu et al., 2003; Shen et al., 2017; Thiry, 2000). However, in our study, the increase in the kaolinite content may be derived from detrital input from old sedimentary sequences in the catchment. By further considering the inverse relation between the total smectite and illite, as well as chlorite, and the generally positive relation between illite and chlorite (Figure 6), we thus chose (smectite+I/S mixed layers)/(illite+chlorite) and (smectite+I/S mixed layers)/illite to identify the changes in the weathering conditions at catchment scale.

Arid conditions and duration for chemical weathering are the two potential factors to influence clay mineral assemblages. In northeastern TP, erosion rates and sediment accumulation rates are higher due to widespread tectonic activities at ~8–9 Ma (Fang et al., 2016; Lease et al., 2007; Li et al., 2014; Zheng et al., 2006, 2010). In the MJZ section, uplift of the northern Dabanshan Mountains at ~8.6 Ma led to higher sedimentation rates (R. S. Yang, Fang, et al., 2017), indicating a faster erosion rate and thus less duration time for chemical weathering. Therefore, the sharp decreases of the total smectite/(illite+chlorite) and total smectite/illite ratios and the content of total smectite at ~7.8 Ma may be also influenced by faster erosion induced by uplift of the Dabanshan Mountains. However, the lag time of ~1 Ma between tectonic uplift (~8.6 Ma) and clay mineral evolution (accelerating at ~7.8 Ma) is too long to link the evolution of the clay assemblage to a change in the duration of chemical weathering. If the duration for weathering was the primary factor, the near-simultaneous appearances of uplift and clay minerals change should be expected. The duration time is thus assumed to play a minor role, which might be due to a weathering regime being already kinetically limited (e.g., West et al., 2005) by the time of the initiation of the deposition at the base of the MJZ section related to an overall tectonically active pattern (relatively high erosion) on the northeastern TP (Li et al., 2014). So clay mineral transition at ~7.8 Ma was primarily controlled by climatic drying with minor influence from shorter duration for chemical weathering.

The ratios of the total smectite/(illite+chlorite) and total smectite/illite and the content of total smectite exhibit long-term slight decreases from ~12.7 to 7.8 Ma and significantly decline at 7.8 Ma toward the range of clay minerals from Pliocene and modern eolian deposition, indicating a rather gradual aridification in this region since ~12.7 Ma and enhanced aridification since 7.8 Ma. As we have mentioned above, smectite is formed in warmer and wetter environments compared with illite. Generally, compared with dominant total smectite (33.5% on average) and illite (45.1% on average) in Pliocene and Quaternary eolian deposits in the Xining Basin, the dominant total smectite (50.8% on average) and illite (34.6% on average) in the MJZ section indicate that the climate was relatively warmer and more humid than the present climate (Figure 11). When combining the younger HW red clay to the MJZ top loess and the evolution of clay minerals, the Xining Basin displays a continuous aridification trend since ~7.8 Ma. The strong agreement between the eolian and fluvial records suggests that clay minerals correspond to the very fine product of the regional erosion and weathering controlled by climate change, and as such they can reflect a broad source area condition regardless of the specific transport agent (wind or river). For the older period, two wetting intervals occurred in ~11.1–10.5 and ~9–7.8 Ma superimposed to the long-term aridification since 12.7 Ma (Figure 5).

Clay minerals are usually formed slowly for several centuries to several million years (Meunier, 2005), and thus clay minerals are not sensitive to precipitation of seasonal variation. Therefore, aridification reconstructed by clay minerals may represent a decrease of precipitation amount. This is supported by the rise in the xerophytic plants and the almost disappearance of aquatic plants at ~8 Ma across the northeastern TP that also indicate decreased precipitation amount (J. Liu, Li, et al., 2016; Ma et al., 1998, 2005; Miao et al., 2012). However, we cannot exclude the possible intensified precipitation seasonality which may be induced by tectonic uplift-driven intensified East Asia monsoon (e.g., X. D. Liu et al., 2015). The intensified drying event at ~7.8 Ma in the Xining Basin is highly consistent with other climatic and sedimentary records from adjacent regions (Figure 12). Clay mineral assemblages from the Japan Sea show an abrupt change at ~8 Ma, indicating that intensified drying of central Asia occurred at that time (Shen et al., 2017). Palynological evidence from the nearby Qaidam Basin (Miao et al., 2012), Jiuquan Basin (Ma et al., 2005), Linxia Basin (Ma et al., 1998), and Tianshui Basin (Hui et al., 2011; J. Liu, Li, et al., 2016) show replacement of forest by steppe at 8, 8.5, 8.4, and 7.4 Ma, respectively. Meanwhile, previous studies have also revealed enhanced aridification events in the northeastern TP and its adjacent regions at approximately 8 Ma using geochemical (Wan et al., 2010; Y. B. Yang, Galy, et al., 2017) and grain size (Fan et al., 2006) records.

At ~8 Ma, the onset of eolian red clay accumulation occurred in the CLP (An et al., 2001; Ding et al., 2001; Qiang et al., 2001), and there was a notable increase in eolian input to the northeastern TP (Guo et al., 2002; Y. B. Yang, Galy, et al., 2017), the North Pacific (Rea et al., 1998), the South China Sea (Wan et al., 2007), and the Japan Sea (Shen et al., 2017), indicating enhanced aridification in central Asia and/or more dust available on the source areas (e.g., Nie et al., 2018). Magnetic enhancements could also be seen in the Qaidam Basin (Nie et al., 2017), the Jianzha Basin (Fu et al., 2017), the Xining Basin (Zan et al., 2018), the Linxia Basin (Yan et al., 2014), and the CLP (Nie et al., 2018) at ~8 Ma, yet the mechanisms of this enhancement are still debated. Eolian dust input (Fu et al., 2017; Nie et al., 2018), provenance change (Yan et al., 2014),



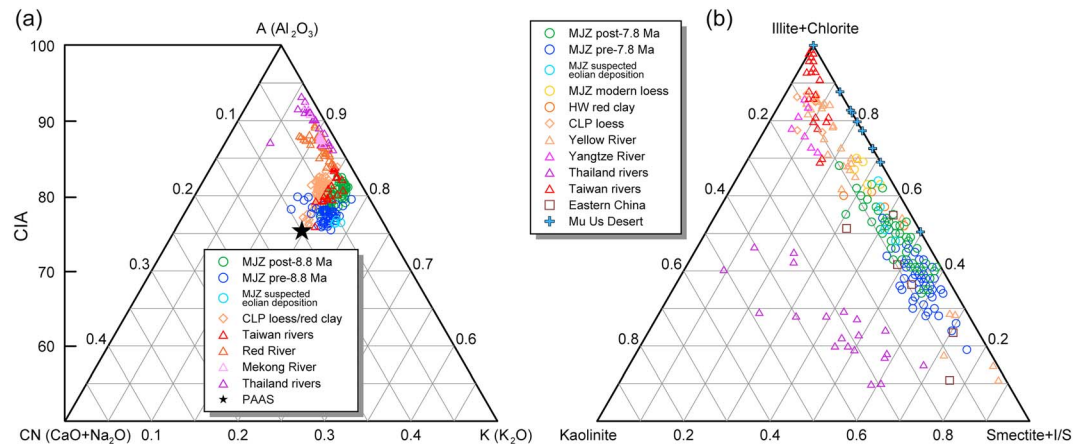


**Figure 11.** (a) Major element  $\text{Al}_2\text{O}_3$ -( $\text{CaO} + \text{Na}_2\text{O}$ )- $\text{K}_2\text{O}$  (A-CN-K) ternary diagram of the  $<2\text{-}\mu\text{m}$  fraction of the MJZ section sediments,  $<5\text{-}\mu\text{m}$  fraction of typical loess and red clays in the CLP (S. F. Xiong et al., 2010),  $<2\text{-}\mu\text{m}$  fraction of sediments in the Red and Mekong Rivers, Thailand rivers, and Taiwan rivers (Z. F. Liu, Zhao, et al., 2016). (b) Ternary diagram of major clay mineral groups (illite + chlorite)-kaolinite-smectite showing variation in clay mineral composition of the MJZ section, loess from the CLP (Shen et al., 2017; Shi et al., 2015), mu Us Desert (Niu et al., 2015), eastern China (Du et al., 2012), Yellow River (S. F. Liu et al., 2014; Pang et al., 2018; Shen et al., 2017), Yangtze River (S. F. Liu et al., 2014; Shen et al., 2017; Wan et al., 2007), Thailand rivers (Z. F. Liu, Zhao, et al., 2016), and Taiwan rivers (Z. F. Liu et al., 2010; Shen et al., 2017). MJZ = Mojiazhuang; CLP = Chinese Loess Plateau; PAAS = Post-Archaean average Australian Shale.

and pedogenic enhancement (Zan et al., 2018) are all thought to be the main potential factors. Despite multiple mechanisms, such modifications may reflect complex responses of fluvial and atmospheric systems to climate-tectonic coupling at  $\sim 8$  Ma on the northeastern TP and the CLP (e.g., Nie et al., 2018). Anyway, the drying event starting at  $\sim 7.8$  Ma reconstructed by clay minerals in the Xining Basin manifests an intensified central Asian aridification event. The long-term drying trend since  $\sim 7.8$  Ma,

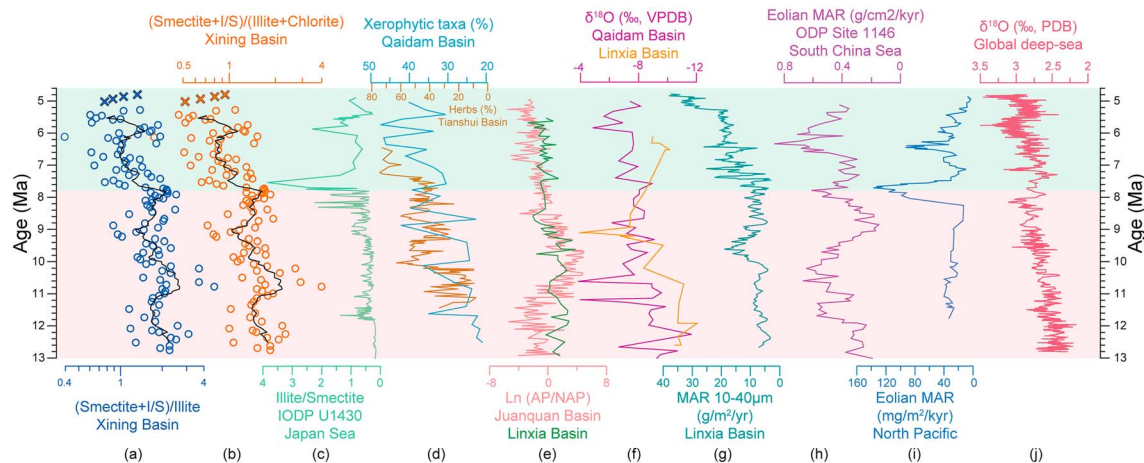


**Figure 12.** Terrestrial and marine records in the late Miocene showing global climate change, climatic aridification, and uplift of the northern Tibetan Plateau. (a, b) (smectite+I/S)/(illite+chlorite) and (I/S mixed layer)/illite ratios showing enhanced aridification at  $\sim 7.8$  Ma in the Xining Basin (this study); (c) illite/smectite ratio at IODP Site U1430 in the Japan Sea (Shen et al., 2017); (d) contents of xerophytic taxa and herbs in the Qaidam Basin (Miao et al., 2012) and the Tianshui Basin (J. Liu, Li, et al., 2016); (e) ratio of arbor to nonarbor trees (AP/NAP) in the Jiuquan and Tianshui basins (Li et al., 2014); (f) oxygen isotope from pedogenic and lacustrine carbonates in the Qaidam Basin (Zhuang et al., 2011) and the Linxia Basin (Fan et al., 2007); (g) eolian sediment mass accumulation rates (MAR) in the Linxia Basin showing intensification of the Asian winter monsoon (Fan et al., 2006); (h, i) eolian MAR at ODP Site 1146 in the South China Sea (Wan et al., 2007) and ODP Site 885/886 in the North Pacific (Rea et al., 1998); (j) compiled global deep-sea  $\delta^{18}\text{O}$  values (Zachos et al., 2001). I/S = illite/smectite; IODP = Integrated Ocean Drilling Program; ODP = Ocean Drilling Program.

constrained by clay minerals of the MJZ section together with eolian deposition in the Xining Basin, suggests that the modern pattern of climate was initiated at that time.

### 5.5. The Driving Mechanisms

The main drivers of the central Asia aridification in the late Cenozoic have long been debated. The retreat of the Paratethys (Ramstein et al., 1997; Z. S. Zhang et al., 2007), global cooling (Ding et al., 2005; Lu & Guo, 2014), and uplift of the TP (Kutzbach et al., 1989; Manabe & Terpstra, 1974; Tada et al., 2016) are considered to be three major drivers accounting for this dramatic change. Here we compare the history and timing of major climatic and tectonic events from global and regional records with our record to explore the main drivers and mechanisms.

Previous studies have proven that the westward retreat of the Paratethys in the Cenozoic, especially from the late Eocene to the late Oligocene, had a significant contribution to the central Asia aridification (Bosboom, et al., 2014a; Carrapa et al., 2015; Ramstein et al., 1997; Sun et al., 2015, 2016; Z. S. Zhang et al., 2007). However, the retreat of the Paratethys from the Tarim Basin should be earlier than the Oligocene, although the exact timing of the regression of seawater from the Tarim Basin is still uncertain (Bosboom, et al., 2014a, 2014b; Carrapa et al., 2015; Sun et al., 2015, 2017). Hence, the retreat of the Paratethys is expected to have a very limited influence on the studied period (since ~12.7 Ma).

Global cooling is considered to be an important factor that led to Asian drying through the strengthening of the winter Siberian High, the reduction of moisture level, and the increase in continental surface area by the of sea level (Ding et al., 2005; Lu & Guo, 2014). After the end of the Middle Miocene Climatic Optimum at ~15 Ma, the Middle Miocene Climatic Cooling occurred, characterized by an abrupt average temperature drop of more than 5 °C and the development of the East Antarctic ice sheet (Flower & Kennett, 1994; Holbourn et al., 2014; Lewis et al., 2008). The global temperature, constrained by the marine benthic  $\delta^{18}\text{O}$  record, continued to slightly drop between the late Miocene and early Pliocene with the development of small-scale ice sheet expansion in the West Antarctic and the Arctic (Zachos et al., 2001). However, we noticed that the benthic  $\delta^{18}\text{O}$  values between ~7.9 and 7.2 Ma are lower than the values in 8–9 Ma, suggesting the global temperature tended to increase rather than decrease in this period (Figure 12). Another global sea surface temperature record showed a global cooling event only starting at ~7 Ma (Herbert et al., 2016). Thus, global cooling was not the trigger of the intensification of aridification at ~7.8 Ma in the Xining Basin, while global cooling may have contributed after ~7 Ma.

Intensified aridification in central Asia may also be induced by the uplift of the TP, which blocked moisture from the ocean, reorganized Asian atmospheric circulation, and enhanced the heating difference between land and ocean (Kutzbach et al., 1989; Li & Fang, 1999; X. D. Liu & Yin, 2002; Manabe & Terpstra, 1974; Tada et al., 2016). Uplift of the different parts of the TP is diachronous. Major uplift of the northeastern TP started from the Miocene, later than the uplift of the southern and central TP (Li et al., 2014; X. H. Liu, Xu, & Ding, 2016). Changes in sedimentary facies and the appearance of conglomerates together with changes in the sedimentation rate in the MJZ section indicate tectonic uplift of the northern boundary of the Xining Basin (the Dabanshan Mountains) at ~8.6 Ma (Figure 13; R. S. Yang, Fang, et al., 2017). On the other part of the northeastern TP, increase in sedimentation rate also occurred at ~8 Ma (Figure 13) in the western Qaidam Basin (Fang et al., 2007), the Guide Basin (Li et al., 2014) and the Linxia Basin (Fang et al., 2016). Rapid exhumation occurred across the northeastern TP between 10 and 7 Ma, specifically in the Altyn Tagh (Z. L. Chen et al., 2002), the Haiyuan Fault (Duvall et al., 2013), the north Qilianshan Mountains (Zheng et al., 2010), the Lajishan Mountains (Lease et al., 2007), the Liupanshan Mountains (Zheng et al., 2003), and the Jishishan Mountains (Zheng et al., 2006). At the same time, the Qaidam Basin and the Linxia Basin underwent significant rotation (Figure 13; Fang et al., 2016). Moreover, the  $\varepsilon_{\text{Nd}}$  in sediments in the Linxia Basin (Y. B. Yang, Galy, et al., 2017), the CLP (Z. Chen & Li, 2013), the Japan Sea (Shen et al., 2017), and the North Pacific (Pettke et al., 2000, 2002; W. F. Zhang, Chen, et al., 2016) collectively display a remarkable change at approximately 8–9 Ma (Figure 13), implying a significant provenance change in the regional riverine and windblown sediments due to tectonic uplift of the northeastern TP. The rapid exhumation in the northern TP associated with the aridification is likely to have led to a greater production of dust, with the concomitance of higher altitude and aridity more favorable to eolian erosion and the transport of dust to the Linxia Basin, the CLP, the Japan Sea, and the North Pacific. However, in the MJZ section, climate proxies lag behind provenance proxies about 1 Myr. This

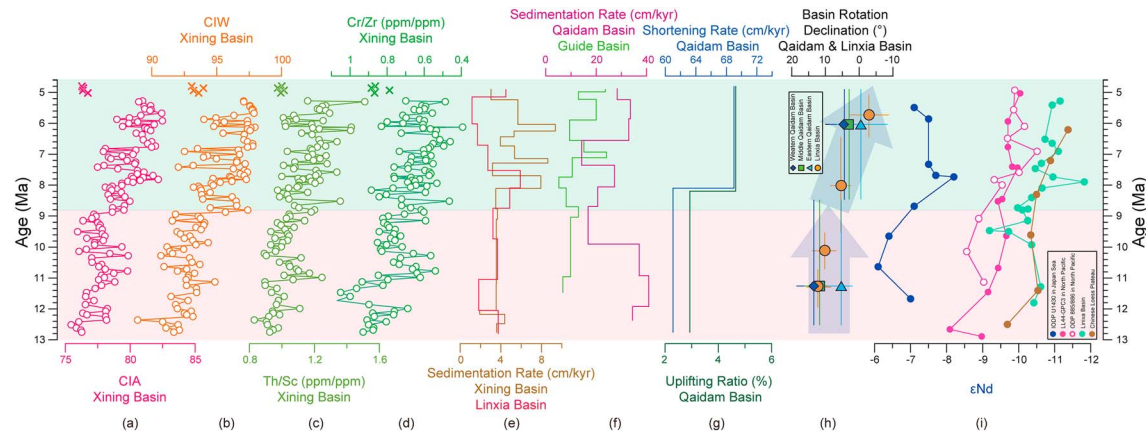


**Figure 13.** (a–d) CIA, CIW, Th/Sc, and Cr/Zr ratios showing provenance change at ~8.8 Ma in the Xining Basin (this study) and their comparison with (e, f) sedimentation rates of the Xining Basin (R. S. Yang, Fang, et al., 2017), the Linxia Basin (Fang et al., 2016), the Qaidam Basin (Fang et al., 2007), and the Guide Basin (Li et al., 2014); (g) average uplifted ratio based on four restorations of seismic profiles in the southern Qaidam Basin (Mao et al., 2014) and average shortening rates of the entire Qaidam Basin (Bao et al., 2017); (h) basin rotation based on paleomagnetic declination in the Linxia and Qaidam Basins (Li et al., 2014); (i)  $\epsilon\text{Nd}(0)$  values of acetic residue of bulk sediments in the Linxia Basin (Y. B. Yang, Galy, et al., 2017), 28- to 45- $\mu\text{m}$  fraction of Chinese Loess Plateau (Z. Chen & Li, 2013), bulk sediments in the IODP Site U1430 in the Japan Sea (Shen et al., 2017), North Pacific bulk sediments in the ODP Site 885/886 (Pettke et al., 2000), and core LL44-GPC3 (Pettke et al., 2002; W. F. Zhang, Chen, et al., 2016). CIA = chemical index of alteration; CIW = chemical index of weathering; IODP = Integrated Ocean Drilling Program; ODP = Ocean Drilling Program.

time lag may correspond to the time needed to establish a new stable state of climate after the tectonic uplift of the Dabanshan Mountains (~8.6 Ma). Therefore, temporally and spatially concurrent climate and tectonic proxies in the Xining Basin, together with other regional climatic and tectonic records, clearly show that the uplift of the northeastern TP was the primary driver that influenced the regional climate since the late Miocene. The uplift of the northeastern TP has forced the regional climate and landscape to approach a new regime during which the deteriorated ambient temperature and moisture conditions and short duration of soil development will yield a reduced intensity of catchment silicate weathering.

## 6. Conclusions

Clay minerals in the MJZ sequence are characterized by dominant I/S mixed layers and illite, with minor kaolinite, chlorite, and smectite. Clay minerals of the MJZ section are all detrital and record limited influence from provenance change. Provenance changes at ~8.8 Ma caused by the uplift of the northern Dabanshan Mountains exhibited a primary control of the commonly used geochemical weathering indexes. The clay mineral assemblages show that a long-term gradual aridification between 12.7 and 4.8 Ma and an enhanced drying since ~7.8 Ma occurred in the Xining Basin. Temporally and spatially concurrent climate and tectonic proxies in the Xining Basin, together with other regional climatic and tectonic records, show that the uplift of the northeastern TP was the major driver of the evolution of the regional climate since the late Miocene and further drove the regional landscape and climate to the modern regime.

## References

- Ahn, J. H., & Peacor, D. R. (1986). Transmission and analytical electron microscopy of the smectite-to-illite transition. *Clays and Clay Minerals*, 34(2), 165. <https://doi.org/10.1346/CCMN.1986.0340207>
- An, Z. S., Kutzbach, J. E., Prell, W. L., & Porter, S. C. (2001). Evolution of Asian monsoons and phased uplift of the Himalaya-Tibetan Plateau since late Miocene times. *Nature*, 411, 62–66. <https://doi.org/10.1038/35075035>
- Aoyagi, K., & Kazama, T. (1980). Transformational changes of clay minerals, zeolites and silica minerals during diagenesis. *Sedimentology*, 27(2), 179–188. <https://doi.org/10.1111/j.1365-3091.1980.tb01168.x>
- Bao, J., Wang, Y. D., Song, C. H., Feng, Y., Hu, C. H., Zhong, S. R., & Yang, J. W. (2017). Cenozoic sediment flux in the Qaidam Basin, northern Tibetan Plateau, and implications with regional tectonics and climate. *Global and Planetary Change*, 155, 56–69. <https://doi.org/10.1016/j.gloplacha.2017.03.006>
- Biscaye, P. E. (1965). Mineralogy and sedimentation of recent deep-sea clay in the Atlantic Ocean and adjacent seas and oceans. *Geological Society of America Bulletin*, 76(7), 803–832. [https://doi.org/10.1130/0016-7606\(1965\)76\[803:MASORD\]2.0.CO;2](https://doi.org/10.1130/0016-7606(1965)76[803:MASORD]2.0.CO;2)

### Acknowledgments

This work was financially supported by the Strategic Priority Research Program (grant XDA20070201), External Cooperation Program (grant 131C11KYSB20160072), and the Youth Innovation Promotion Association (grant 2018095) of the Chinese Academy of Sciences, the National Natural Science Foundation of China (grants 41771236 and 41620104002). R. S. Yang is supported by the China Scholarship Council. We would like to thank Xiaohui Fang, Shuang Lv, Haichao Guo, Yulong Xie, Ziqiang Mao, Shengcheng Lu, Jian Kang, Wenyuan Han, Zhenyu Wang, and Yong Xue for their assistance in the field and laboratory. Data used in this study are available in the online supporting information.

- Bosboom, R., Dupont-Nivet, G., Grothe, A., Brinkhuis, H., Villa, G., Mandic, O., et al. (2014a). Linking Tarim Basin sea retreat (west China) and Asian aridification in the late Eocene. *Basin Research*, 26(5), 621–640. <https://doi.org/10.1111/bre.12054>
- Bosboom, R., Dupont-Nivet, G., Grothe, A., Brinkhuis, H., Villa, G., Mandic, O., et al. (2014b). Timing, cause and impact of the late Eocene stepwise sea retreat from the Tarim Basin (west China). *Palaeogeography, Palaeoclimatology, Palaeoecology*, 403, 101–118. <https://doi.org/10.1016/j.palaeo.2014.03.035>
- Bosboom, R. E., Abels, H. A., Hoon, C., van den Berg, B. C., Guo, Z., & Dupont-Nivet, G. (2014). Aridification in continental Asia after the Middle Eocene Climatic Optimum (MECO). *Earth and Planetary Science Letters*, 389, 34–42. <https://doi.org/10.1016/j.epsl.2013.12.014>
- Bouquillon, A., France-Lanord, C., Michard, A., & Tiercelin, J.-J. (1990). Sedimentology and isotopic chemistry of the Bengal Fan sediments: the denudation of the Himalaya. In J. R. Cochran et al. (Eds.), *Proceedings of the Ocean Drilling Program, Scientific Results* (Vol. 116, pp. 43–58). College Station, TX: Texas A&M University.
- Carrapa, B., DeCelles, P. G., Wang, X., Clementz, M. T., Mancin, N., Stoica, M., et al. (2015). Tectono-climatic implications of Eocene Paratethys regression in the Tajik basin of central Asia. *Earth and Planetary Science Letters*, 424, 168–178. <https://doi.org/10.1016/j.epsl.2015.05.034>
- Caves, J. K., Moragne, D. Y., Ibarra, D. E., Bayshashov, B. U., Gao, Y., Jones, M. M., et al. (2016). The Neogene de-greening of central Asia. *Geology*, 44(11), 887–890. <https://doi.org/10.1130/G38267.1>
- Chamley, H. (1989). *Clay sedimentology*. Berlin, Heidelberg: Springer-Verlag. <https://doi.org/10.1007/978-3-642-85916-8>
- Chamley, H. (1994). Clay mineral diagenesis. In A. Parker & B. W. Sellwood (Eds.), *Quantitative diagenesis: Recent developments and applications to reservoir geology* (pp. 161–188). Netherlands: Springer. [https://doi.org/10.1007/978-94-011-0189-9\\_5](https://doi.org/10.1007/978-94-011-0189-9_5)
- Chen, Q., Liu, Z. F., & Kissel, C. (2017). Clay mineralogical and geochemical proxies of the East Asian summer monsoon evolution in the South China Sea during Late Quaternary. *Scientific Reports*, 7(1), 42,083. <https://doi.org/10.1038/srep42083>
- Chen, Z., & Li, G. J. (2013). Evolving sources of eolian detritus on the Chinese Loess Plateau since early Miocene: Tectonic and climatic controls. *Earth and Planetary Science Letters*, 371, 220–225. <https://doi.org/10.1016/j.epsl.2013.03.044>
- Chen, Z. L., Wan, J. L., Wang, X. F., Chen, X. H., & Pan, J. H. (2002). Rapid strike-slip of the Altyn Tagh fault at 8 Ma and its geological implications [in Chinese with English abstract]. *Acta Geologica Sinica*, 23, 295–300.
- Chi, Y. P., Fang, X. M., Song, C. H., Miao, Y. F., Teng, X. H., Han, W. X., et al. (2013). Cenozoic organic carbon isotope and pollen records from the Xining Basin, NE Tibetan Plateau, and their palaeoenvironmental significance. *Palaeogeography, Palaeoclimatology, Palaeoecology*, 386, 436–444. <https://doi.org/10.1016/j.palaeo.2013.06.013>
- Clift, P. D., Wan, S. M., & Blusztajn, J. (2014). Reconstructing chemical weathering, physical erosion and monsoon intensity since 25 Ma in the northern South China Sea: A review of competing proxies. *Earth-Science Reviews*, 130, 86–102. <https://doi.org/10.1016/j.earscirev.2014.01.002>
- Court, J. E., Goldman, C. R., & Hyne, N. J. (1972). Surface sediments in Lake Tahoe, California-Nevada. *Journal of Sedimentary Research*, 42(2), 359–377. <https://doi.org/10.1306/74D72554-2B21-11D7-8648000102C1865D>
- Cullers, R. L. (1994). The chemical signature of source rocks in size fractions of Holocene stream sediment derived from metamorphic rocks in the Wet Mountains region, Colorado, U.S.A. *Chemical Geology*, 113(3–4), 327–343. [https://doi.org/10.1016/0009-2541\(94\)90074-4](https://doi.org/10.1016/0009-2541(94)90074-4)
- Dai, S., Fang, X. M., Dupont-Nivet, G., Song, C. H., Gao, J. P., Krijgsman, W., et al. (2006). Magnetostratigraphy of Cenozoic sediments from the Xining Basin: Tectonic implications for the northeastern Tibetan Plateau. *Journal of Geophysical Research*, 111, B11102. <https://doi.org/10.1029/2005JB004187>
- Ding, Z. L., Derbyshire, E., Yang, S. L., Sun, J. M., & Liu, T. S. (2005). Stepwise expansion of desert environment across northern China in the past 3.5 Ma and implications for monsoon evolution. *Earth and Planetary Science Letters*, 237(1–2), 45–55. <https://doi.org/10.1016/j.epsl.2005.06.036>
- Ding, Z. L., Yang, S. L., Hou, S. S., Wang, X., Chen, Z., & Liu, T. S. (2001). Magnetostratigraphy and sedimentology of the Jingchuan red clay section and correlation of the Tertiary eolian red clay sediments of the Chinese Loess Plateau. *Journal of Geophysical Research*, 106(B4), 6399–6407. <https://doi.org/10.1029/2000JB900445>
- Du, K., Chen, Y., Ji, J. F., Li, H., Long, X. Y., & Chen, J. (2012). Characteristics of clay minerals and CO<sub>2</sub> consumption rates of weathering profiles from Cenozoic basalts in eastern China [in Chinese with English abstract]. *Geological Journal of China Universities*, 18(2), 256–272.
- Ducloux, J., Meunier, A., & Velde, B. (1976). Smectite, chlorite and a regular interlayered chlorite-vermiculite in soils developed on a small serpentinite body, Massif Central, France. *Clay Minerals*, 11(02), 121–135. <https://doi.org/10.1180/claymin.1976.011.2.04>
- Dunoyer de Segonzac, G. (1970). The transformation of clay minerals during diagenesis and low-grade metamorphism: A review. *Sedimentology*, 10, 137–143. <https://doi.org/10.1111/j.1365-3091.1970.tb02190.x>
- Dupont-Nivet, G., Krijgsman, W., Langereis, C. G., Abels, H. A., Dai, S., & Fang, X. M. (2007). Tibetan Plateau aridification linked to global cooling at the Eocene–Oligocene transition. *Nature*, 445(7128), 635–638. <https://doi.org/10.1038/nature05516>
- Duvall, A. R., Clark, M. K., Kirby, E., Farley, K. A., Craddock, W. H., Li, C., & Yuan, D.-Y. (2013). Low-temperature thermochronometry along the Kunlun and Haiyuan faults, NE Tibetan Plateau: Evidence for kinematic change during late-stage orogenesis. *Tectonics*, 32, 1190–1211. <https://doi.org/10.1002/tect.20072>
- Fagel, N. (2007). Chapter four clay minerals, deep circulation and climate. *Developments in Marine Geology*, 1, 139–184. [https://doi.org/10.1016/S1572-5480\(07\)01009-3](https://doi.org/10.1016/S1572-5480(07)01009-3)
- Fan, M. J., Dettman, D. L., Song, C. H., Fang, X. M., & Garzzone, C. N. (2007). Climatic variation in the Linxia basin, NE Tibetan Plateau, from 13.1 to 4.3 Ma: The stable isotope record. *Palaeogeography, Palaeoclimatology, Palaeoecology*, 247(3–4), 313–328. <https://doi.org/10.1016/j.palaeo.2006.11.001>
- Fan, M. J., Song, C. H., Dettman, D. L., Fang, X. M., & Xu, X. H. (2006). Intensification of the Asian winter monsoon after 7.4 Ma: Grain-size evidence from the Linxia Basin, northeastern Tibetan Plateau, 13.1 Ma to 4.3 Ma. *Earth and Planetary Science Letters*, 248(1–2), 186–197. <https://doi.org/10.1016/j.epsl.2006.05.025>
- Fang, X. M., Wang, J. Y., Zhang, W. L., Zan, J. B., Song, C. H., Yan, M. D., et al. (2016). Tectonosedimentary evolution model of an intracontinental flexural (foreland) basin for paleoclimatic research. *Global and Planetary Change*, 145, 78–97. <https://doi.org/10.1016/j.gloplacha.2016.08.015>
- Fang, X. M., Zhang, W. L., Meng, Q. Q., Gao, J. P., Wang, X. M., King, J., et al. (2007). High-resolution magnetostratigraphy of the Neogene Huaitoutala section in the eastern Qaidam Basin on the NE Tibetan Plateau, Qinghai Province, China and its implication on tectonic uplift of the NE Tibetan Plateau. *Earth and Planetary Science Letters*, 258(1–2), 293–306. <https://doi.org/10.1016/j.epsl.2007.03.042>
- Fedo, C. M., Nesbitt, H. W., & Young, G. M. (1995). Unraveling the effects of potassium metasomatism in sedimentary rocks and paleosols, with implications for paleoweathering conditions and provenance. *Geology*, 23(10), 921–924. [https://doi.org/10.1130/0091-7613\(1995\)023<0921:UTEOPM>2.3.CO;2](https://doi.org/10.1130/0091-7613(1995)023<0921:UTEOPM>2.3.CO;2)



- Flower, B. P., & Kennett, J. P. (1994). The middle Miocene climatic transition: East Antarctic ice sheet development, deep ocean circulation and global carbon cycling. *Palaeogeography, Palaeoclimatology, Palaeoecology*, *108*(3–4), 537–555. [https://doi.org/10.1016/0031-0182\(94\)90251-8](https://doi.org/10.1016/0031-0182(94)90251-8)
- Fu, C. F., Qiang, X. K., Xu, X. W., Xi, J. W., Zuo, J., & An, Z. S. (2017). Late Miocene magnetostratigraphy of Jianzha Basin in the north-eastern margin of the Tibetan Plateau and changes in the East Asian summer monsoon. *Geological Journal*, *53*, 282–292. <https://doi.org/10.1002/gj.3047>
- Gao, X. (2017). *Clay mineralogy [in Chinese]*. Beijing: Chemical Industry Press.
- Guo, Z. T., Ruddiman, W. F., Hao, Q. Z., Wu, H. B., Qiao, Y. S., Zhu, R. X., et al. (2002). Onset of Asian desertification by 22 Myr ago inferred from loess deposits in China. *Nature*, *416*(6877), 159–163. <https://doi.org/10.1038/416159a>
- Gylesjö, S., & Arnold, E. (2006). Clay mineralogy of a red clay-loess sequence from Lingtai, the Chinese Loess Plateau. *Global and Planetary Change*, *51*(3–4), 181–194. <https://doi.org/10.1016/j.gloplacha.2006.03.002>
- Han, J. E., Shao, Z. G., Chen, Q. G., Meng, X. G., Zhu, D. G., Zhang, Q., et al. (2015). Discovery and significance of *Hipparion* and *Parelasomotherium* fossils in the Xining Basin, Qinghai Province [in Chinese with English abstract]. *Acta Geologica Sinica*, *36*, 115–120. <https://doi.org/10.3975/cagsb.2015.01.14>
- Harnois, L. (1988). The CIW index: A new chemical index of weathering. *Sedimentary Geology*, *55*(3–4), 319–322. [https://doi.org/10.1016/0037-0738\(88\)90137-6](https://doi.org/10.1016/0037-0738(88)90137-6)
- Harris, N. (2006). The elevation history of the Tibetan Plateau and its implications for the Asian monsoon. *Palaeogeography Palaeoclimatology Palaeoecology*, *241*(1), 4–15. <https://doi.org/10.1016/j.palaeo.2006.07.009>
- Herbert, T. D., Lawrence, K. T., Tzanova, A., Peterson, L. C., Caballero-Gill, R., & Kelly, C. S. (2016). Late Miocene global cooling and the rise of modern ecosystems. *Nature Geoscience*, *9*(11), 843–847. <https://doi.org/10.1038/ngeo2813>
- Hillier, S. (1995). Erosion, sedimentation and sedimentary origin of clays. In *Origin and mineralogies of clays* (Ed. by B. Velde), pp. 162–219. Springer-Verlag, Berlin
- Holbourn, A., Kuhnt, W., Lyle, M., Schneider, L., Romero, O., & Andersen, N. (2014). Middle Miocene climate cooling linked to intensification of eastern equatorial Pacific upwelling. *Geology*, *42*(1), 19–22. <https://doi.org/10.1130/G34890.1>
- Hong, H. L., Fang, Q., Wang, C. W., Churchman, G. J., Zhao, L. L., Gong, N. N., & Yin, K. (2017). Clay mineralogy of altered tephra beds and facies correlation between the Permian-Triassic boundary stratigraphic sets, Guizhou, South China. *Applied Clay Science*, *143*, 10–21. <https://doi.org/10.1016/j.clay.2017.03.014>
- Hong, H. L., Li, Z. H., Xue, H. J., Zhu, Y. H., Zhang, K. X., & Xiang, S. Y. (2007). Oligocene clay mineralogy of the Linxia Basin: Evidence of paleoclimatic evolution subsequent to the initial-stage uplift of the Tibetan Plateau. *Clays and Clay Minerals*, *55*(5), 491–503. <https://doi.org/10.1346/CCMN.2007.0550504>
- Hong, H. L., Zhang, K. X., & Li, Z. H. (2010). Climatic and tectonic uplift evolution since ~7 Ma in Gyirong basin, southwestern Tibet Plateau: Clay mineral evidence. *International Journal of Earth Sciences*, *99*(6), 1305–1315. <https://doi.org/10.1007/s00531-009-0457-x>
- Horton, B. K., Dupont-Nivet, G., Zhou, J., Waanders, G. L., Butler, R. F., & Wang, J. (2004). Mesozoic-Cenozoic evolution of the Xining-Minhe and Dangchang basins, northeastern Tibetan Plateau: Magnetostratigraphic and biostratigraphic results. *Journal of Geophysical Research*, *109*, B04402. <https://doi.org/10.1029/2003JB002913>
- Hower, J., Eslinger, E. V., Hower, M. E., & Perry, E. A. (1976). Mechanism of burial metamorphism of argillaceous sediment: 1. Mineralogical and chemical evidence. *Geological Society of America Bulletin*, *87*(5), 725–737. [https://doi.org/10.1130/0016-7606\(1976\)87<725:MOBMOA>2.0.CO;2](https://doi.org/10.1130/0016-7606(1976)87<725:MOBMOA>2.0.CO;2)
- Huang, B. C., Piper, J. D. A., Peng, S. T., Liu, T., Li, Z., Wang, Q. C., & Zhu, R. X. (2006). Magnetostratigraphic study of the Kuche Depression, Tarim Basin, and Cenozoic uplift of the Tian Shan range, western China. *Earth and Planetary Science Letters*, *251*(3–4), 346–364. <https://doi.org/10.1016/j.epsl.2006.09.020>
- Hui, Z. C., Li, J. J., Xu, Q. H., Song, C. H., Zhang, J., Wu, F. L., & Zhao, Z. J. (2011). Miocene vegetation and climatic changes reconstructed from a sporopollen record of the Tianshui Basin, NE Tibetan Plateau. *Palaeogeography, Palaeoclimatology, Palaeoecology*, *308*(3–4), 373–382. <https://doi.org/10.1016/j.palaeo.2011.05.043>
- Huyghe, P., Guilbaud, R., Bernet, M., Galy, A., & Gajurel, A. P. (2011). Significance of the clay mineral distribution in fluvial sediments of the Neogene to recent Himalayan foreland basin (west-central Nepal). *Basin Research*, *23*(3), 332–345. <https://doi.org/10.1111/j.1365-2117.2010.00485.x>
- Kemp, S. J., Ellis, M. A., Mountney, I., & Kender, S. (2016). Palaeoclimatic implications of high-resolution clay mineral assemblages preceding and across the onset of the Palaeocene–Eocene thermal maximum, North Sea Basin. *Clay Minerals*, *51*(05), 793–813. <https://doi.org/10.1180/claymin.2016.051.5.08>
- Kutzbach, J. E., Guetter, P. J., Ruddiman, W. F., & Prell, W. L. (1989). Sensitivity of climate to late Cenozoic uplift in southern Asia and the American West: Numerical experiments. *Journal of Geophysical Research*, *94*(D15), 18,393–18,407. <https://doi.org/10.1029/JD094iD15p18393>
- Lease, R. O., Burbank, D. W., Gehrels, G. E., Wang, Z., & Yuan, D. (2007). Signatures of mountain building: Detrital zircon U/Pb ages from northeastern Tibet. *Geology*, *35*(3), 239–242. <https://doi.org/10.1130/G23057A.1>
- Lewis, A. R., Marchant, D. R., Ashworth, A. C., Hedenäs, L., Hemming, S. R., Johnson, J. V., et al. (2008). Mid-Miocene cooling and the extinction of tundra in continental Antarctica. *Proceedings of the National Academy of Sciences*, *105*(31), 10,676–10,680. <https://doi.org/10.1073/pnas.0802501105>
- Li, J. J., & Fang, X. M. (1999). Uplift of the Tibetan Plateau and environmental changes. *Chinese Science Bulletin*, *44*(23), 2117–2124. <https://doi.org/10.1007/BF03182692>
- Li, J. J., Fang, X. M., Song, C. H., Pan, B. T., Ma, Y. Z., & Yan, M. D. (2014). Late Miocene–Quaternary rapid stepwise uplift of the NE Tibetan Plateau and its effects on climatic and environmental changes. *Quaternary Research*, *81*(03), 400–423. <https://doi.org/10.1016/j.yqres.2014.01.002>
- Liang, M. Y., Guo, Z. T., Kahmann, A. J., & Oldfield, F. (2009). Geochemical characteristics of the Miocene eolian deposits in China: Their provenance and climate implications. *Geochemistry, Geophysics, Geosystems*, *10*, Q04004. <https://doi.org/10.1029/2008GC002331>
- Liu, J., Li, J. J., Song, C. H., Yu, H., Peng, T. J., Hui, Z. C., & Ye, X. Y. (2016). Palynological evidence for late Miocene stepwise aridification on the northeastern Tibetan Plateau. *Climate of the Past*, *12*(7), 1473–1484. <https://doi.org/10.5194/cp-12-1473-2016>
- Liu, S. F., Shi, X. F., Fang, X. S., Dou, Y. G., Liu, Y. G., & Wang, X. C. (2014). Spatial and temporal distributions of clay minerals in mud deposits on the inner shelf of the East China Sea: Implications for paleoenvironmental changes in the Holocene. *Quaternary International*, *349*, 270–279. <https://doi.org/10.1016/j.quaint.2014.07.016>

- Liu, X. D., Sun, H., Miao, Y. F., Dong, B. W., & Yin, Z.-Y. (2015). Impacts of uplift of northern Tibetan Plateau and formation of Asian inland deserts on regional climate and environment. *Quaternary Science Reviews*, *116*, 1–14. <https://doi.org/10.1016/j.quascirev.2015.03.010>
- Liu, X. D., & Yin, Z. Y. (2002). Sensitivity of East Asian monsoon climate to the uplift of the Tibetan Plateau. *Palaeogeography, Palaeoclimatology, Palaeoecology*, *183*(3–4), 223–245. [https://doi.org/10.1016/S0031-0182\(01\)00488-6](https://doi.org/10.1016/S0031-0182(01)00488-6)
- Liu, X. H., Xu, Q., & Ding, L. (2016). Differential surface uplift: Cenozoic paleoelevation history of the Tibetan Plateau. *Science China Earth Sciences*, *59*(11), 2105–2120. <https://doi.org/10.1007/s11430-015-5486-y>
- Liu, Z. F., Colin, C., Li, X. J., Zhao, Y. L., Tuo, S. T., Chen, Z., et al. (2010). Clay mineral distribution in surface sediments of the northeastern South China Sea and surrounding fluvial drainage basins: Source and transport. *Marine Geology*, *277*(1–4), 48–60. <https://doi.org/10.1016/j.margeo.2010.08.010>
- Liu, Z. F., Trentesaux, A., Clemens, S. C., Colin, C., Wang, P. X., Huang, B. Q., & Boulay, S. (2003). Clay mineral assemblages in the northern South China Sea: Implications for East Asian monsoon evolution over the past 2 million years. *Marine Geology*, *201*(1–3), 133–146. [https://doi.org/10.1016/S0025-3227\(03\)00213-5](https://doi.org/10.1016/S0025-3227(03)00213-5)
- Liu, Z. F., Zhao, Y. L., Colin, C., Statterger, K., Wiesner, M. G., Huh, C. A., et al. (2016). Source-to-sink transport processes of fluvial sediments in the South China Sea. *Earth-Science Reviews*, *153*, 238–273. <https://doi.org/10.1016/j.earscirev.2015.08.005>
- Lu, H. Y., & Guo, Z. T. (2014). Evolution of the monsoon and dry climate in East Asia during late Cenozoic: A review. *Science China Earth Sciences*, *57*(1), 70–79. <https://doi.org/10.1007/s11430-013-4790-3>
- Ma, Y. Z., Fang, X. M., Li, J. J., Wu, F. L., & Zhang, J. (2005). The vegetation and climate change during Neocene and Early Quaternary in Jiuxi Basin, China. *Science in China, Series D: Earth Sciences*, *48*(5), 676–688. <https://doi.org/10.1360/03yd0110>
- Ma, Y. Z., Li, J. J., & Fang, X. M. (1998). Records of the climatic variation and pollen flora from the red beds at 30.6–5.0 Ma in Linxia district [in Chinese with English abstract]. *Chinese Science Bulletin*, *43*, 301–304.
- Manabe, S., & Terpstra, T. B. (1974). The effects of mountains on the general circulation of the atmosphere as identified by numerical experiments. *Journal of the Atmospheric Sciences*, *31*(1), 3–42. [https://doi.org/10.1175/1520-0469\(1974\)031<0003:TEOMOT>2.0.CO;2](https://doi.org/10.1175/1520-0469(1974)031<0003:TEOMOT>2.0.CO;2)
- Mao, L. G., Xiao, A. C., Wu, L., Li, B. L., Wang, L. Q., Lou, Q. Q., et al. (2014). Cenozoic tectonic and sedimentary evolution of southern Qaidam Basin, NE Tibetan Plateau and its implication for the rejuvenation of eastern Kunlun Mountains. *Science China Earth Sciences*, *57*(11), 2726–2739. <https://doi.org/10.1007/s11430-014-4951-z>
- McLennan, S. M. (1989). Rare earth elements in sedimentary rocks; influence of provenance and sedimentary processes. *Reviews in Mineralogy and Geochemistry*, *21*(1), 169–200.
- McLennan, S. M., Hemming, S., McDaniel, D. K., & Hanson, G. N. (1993). Geochemical approaches to sedimentation, provenance, and tectonics. *Special Papers-Geological Society of America*, 21–21. <https://doi.org/10.1130/SPE284-p21>
- McMurtry, G. M., & Fan, P. F. (1974). Clays and clay minerals of the Santa Ana River drainage basin, California. *Journal of Sedimentary Research*, *44*(4), 1072–1078. <https://doi.org/10.1306/212F6C35-2B24-11D7-8648000102C1865D>
- Meunier, A. (2005). *Clays*. Berlin: Springer-Verlag.
- Miao, Y. F., Herrmann, M., Wu, F. L., Yan, X. L., & Yang, S. L. (2012). What controlled mid–late Miocene long-term aridification in central Asia?—Global cooling or Tibetan Plateau uplift: A review. *Earth-Science Reviews*, *112*(3–4), 155–172. <https://doi.org/10.1016/j.earscirev.2012.02.003>
- Molnar, P. (2005). Mio-Pliocene growth of the Tibetan Plateau and evolution of East Asian climate. *Palaeontologia Electronica*, *8*(1), 1–23.
- Moore, D. M., & Reynolds, R. C. (1997). *X-ray diffraction and the identification and analysis of clay minerals* (2nd ed.). New York: Oxford University Press.
- Nadeau, P. H., Tait, J. M., McHardy, W. J., & Wilson, M. J. (1984). Interstratified XRD characteristics of physical mixtures of elementary clay particles. *Clay Minerals*, *19*(1), 67. <https://doi.org/10.1180/claymin.1984.019.1.07>
- Nesbitt, H. W., & Young, G. M. (1982). Early Proterozoic climate and plate motions inferred from major element chemistry of lutites. *Nature*, *299*(5885), 715–717. <https://doi.org/10.1038/299715a0>
- Nie, J. S., Garzzone, C., Su, Q. D., Liu, Q. S., Zhang, R., Heslop, D., et al. (2017). Dominant 100,000-year precipitation cyclicality in a late Miocene lake from northeast Tibet. *Science Advances*, *3*(3), e1600762. <https://doi.org/10.1126/sciadv.1600762>
- Nie, J. S., Pullen, A., Garzzone, C. N., Peng, W. B., & Wang, Z. (2018). Pre-Quaternary decoupling between Asian aridification and high dust accumulation rates. *Science Advances*, *4*(2), eaao6977. <https://doi.org/10.1126/sciadv.aao6977>
- Nie, J. S., Stevens, T., Song, Y. G., King, J. W., Zhang, R., Ji, S. C., et al. (2014). Pacific freshening drives Pliocene cooling and Asian monsoon intensification. *Scientific Reports*, *4*(1), 5474. <https://doi.org/10.1038/srep05474>
- Niu, D. F., Li, B. S., Wang, F. N., Wen, X. H., Ma, J. L., & Shu, P. X. (2015). Climate changes indicated by the clay minerals: A case of the Dishaogouwan section on the southeastern margin of the Mu Us Desert [in Chinese with English abstract]. *Journal of Fuzhou University*, *43*(3), 345–351. <https://doi.org/10.7631/issn.1000-2243.2015.03.0345>
- Pang, H. L., Pan, B. T., Garzanti, E., Gao, H. S., Zhao, X., & Chen, D. B. (2018). Mineralogy and geochemistry of modern Yellow River sediments: Implications for weathering and provenance. *Chemical Geology*, *488*, 76–86. <https://doi.org/10.1016/j.chemgeo.2018.04.010>
- Pettke, T., Halliday, A. N., & Rea, D. K. (2002). Cenozoic evolution of Asian climate and sources of Pacific seawater Pb and Nd derived from eolian dust of sediment core LL44-GPC3. *Paleoceanography*, *17*(3), 1031. <https://doi.org/10.1029/2001PA000673>
- Pettke, T., Halliday, A. N., Hall, C. M., & Rea, D. K. (2000). Dust production and deposition in Asia and the North Pacific Ocean over the past 12 Myr. *Earth and Planetary Science Letters*, *178*(3–4), 397–413. [https://doi.org/10.1016/S0012-821X\(00\)00083-2](https://doi.org/10.1016/S0012-821X(00)00083-2)
- Qiang, X. K., Li, Z. X., Powell, C. M., & Zheng, H. B. (2001). Magnetostratigraphic record of the late Miocene onset of the East Asian monsoon, and Pliocene uplift of northern Tibet. *Earth and Planetary Science Letters*, *187*(1–2), 83–93. [https://doi.org/10.1016/S0012-821X\(01\)00281-3](https://doi.org/10.1016/S0012-821X(01)00281-3)
- Qinghai Bureau of Geology and Mineral Resources (QBGMR) (1991). *Regional geology of the Qinghai Province* (pp. 1–662) [in Chinese]]. Beijing, China: Geological Publishing House.
- Ramstein, G., Fluteau, F., Besse, J., & Joussaume, S. (1997). Effect of orogeny, plate motion and land-sea distribution on Eurasian climate change over the past 30 million years. *Nature*, *386*(6627), 788–795. <https://doi.org/10.1038/386788a0>
- Rea, D. K., Snoeckx, H., & Joseph, L. H. (1998). Late Cenozoic eolian deposition in the North Pacific: Asian drying, Tibetan uplift, and cooling of the Northern Hemisphere. *Paleoceanography*, *13*(3), 215–224. <https://doi.org/10.1029/98PA00123>
- Reynolds, R. C. (1980). Interstratified clay minerals. In G. W. Brindley & G. Brown (Eds.), *Crystal structures of clay minerals and their X-ray identification* (pp. 249–303). London: Mineralogical Society. <https://doi.org/10.1180/mono-5.4>
- Ruddiman, W. F., & Kutzbach, J. E. (1989). Forcing of late Cenozoic Northern Hemisphere climate by plateau uplift in southern Asia and the American West. *Journal of Geophysical Research*, *94*(D15), 18,409–18,427. <https://doi.org/10.1029/JD094iD15p18409>

- Schultz, L. S. (1964). *Quantitative interpretation of mineral composition from X-ray and chemical data for the Pierre Shale*. Washington, DC: Geological Survey.
- Shen, X. Y., Wan, S. M., France-Lanord, C., Clift, P. D., Tada, R., Révillon, S., et al. (2017). History of Asian eolian input to the Sea of Japan since 15 Ma: Links to Tibetan uplift or global cooling? *Earth and Planetary Science Letters*, *474*, 296–308. <https://doi.org/10.1016/j.epsl.2017.06.053>
- Shi, Y. X., Dai, X. R., Song, Z. G., Zhang, W. G., & Wang, L. Q. (2005). Characteristics of clay mineral assemblages and their spatial distribution of Chinese loess in different climatic zones [in Chinese with English abstract]. *Acta Sedimentologica Sinica*, *23*(4), 690.
- Singer, A. (1980). The paleoclimatic interpretation of clay minerals in soils and weathering profiles. *Earth-Science Reviews*, *15*(4), 303–326. [https://doi.org/10.1016/0012-8252\(80\)90113-0](https://doi.org/10.1016/0012-8252(80)90113-0)
- Singer, A. (1984). The paleoclimatic interpretation of clay minerals in sediments—A review. *Earth-Science Reviews*, *21*(4), 251–293. [https://doi.org/10.1016/0012-8252\(84\)90055-2](https://doi.org/10.1016/0012-8252(84)90055-2)
- Song, Y. G., Wang, Q. S., An, Z. S., Qiang, X. K., Dong, J. B., Chang, H., et al. (2018). Mid-Miocene Climatic Optimum: Clay mineral evidence from the red clay succession, Longzhong Basin, northern China. *Palaeogeography, Palaeoclimatology, Palaeoecology*, *512*, 46–55. <https://doi.org/10.1016/j.palaeo.2017.10.001>
- Sun, J. M., Gong, Z. J., Tian, Z. H., Jia, Y. Y., & Windley, B. (2015). Late Miocene stepwise aridification in the Asian interior and the interplay between tectonics and climate. *Palaeogeography, Palaeoclimatology, Palaeoecology*, *421*, 48–59. <https://doi.org/10.1016/j.palaeo.2015.01.001>
- Sun, J. M., Liu, W. G., Liu, Z. H., Deng, T., Windley, B. F., & Fu, B. H. (2017). Extreme aridification since the beginning of the Pliocene in the Tarim Basin, western China. *Palaeogeography, Palaeoclimatology, Palaeoecology*, *485*, 189–200. <https://doi.org/10.1016/j.palaeo.2017.06.012>
- Sun, J. M., Windley, B. F., Zhang, Z. L., Fu, B. H., & Li, S. H. (2016). Diachronous seawater retreat from the southwestern margin of the Tarim Basin in the late Eocene. *Journal of Asian Earth Sciences*, *116*, 222–231. <https://doi.org/10.1016/j.jseas.2015.11.020>
- Tada, R., Zheng, H., & Clift, P. D. (2016). Evolution and variability of the Asian monsoon and its potential linkage with uplift of the Himalaya and Tibetan Plateau. *Progress in Earth and Planetary Science*, *3*(1), 4. <https://doi.org/10.1186/s40645-016-0080-y>
- Tapponnier, P., Xu, Z. Q., Roger, F., Meyer, B., Arnaud, N., Wittlinger, G., & Yang, J. S. (2001). Oblique stepwise rise and growth of the Tibet Plateau. *Science*, *294*(5547), 1671–1677. <https://doi.org/10.1126/science.105978>
- Taylor, S. R., & McLennan, S. M. (1985). *The continental crust: Its composition and evolution*. Oxford: Blackwell Scientific Publications.
- Thiry, M. (2000). Palaeoclimatic interpretation of clay minerals in marine deposits: An outlook from the continental origin. *Earth-Science Reviews*, *49*(1–4), 201–221. [https://doi.org/10.1016/S0012-8252\(99\)00054-9](https://doi.org/10.1016/S0012-8252(99)00054-9)
- Tomadin, L., Galignani, P., Landuzzi, V., & Oliveri, F. (1986). Fluvial pelitic supplies from the Apennines to the Adriatic Sea. I—The rivers of the Abruzzo Region. *Mineralogica et Petrographica Acta A*, *29*, 277–286.
- Vanderaverroet, P. (2000). Miocene to Pleistocene clay mineral sedimentation on the New Jersey shelf. *Oceanologica Acta*, *23*(1), 25–36. [https://doi.org/10.1016/S0399-1784\(00\)00102-X](https://doi.org/10.1016/S0399-1784(00)00102-X)
- Wan, S. M., Clift, P. D., Li, A. C., Li, T. G., & Yin, X. B. (2010). Geochemical records in the South China Sea: Implications for East Asian summer monsoon evolution over the last 20 Ma. *Geological Society, London, Special Publications*, *342*(1), 245–263. <https://doi.org/10.1144/SP342.14>
- Wan, S. M., Li, A. C., Clift, P. D., & Stuu, J. B. W. (2007). Development of the East Asian monsoon: Mineralogical and sedimentologic records in the northern South China Sea since 20 Ma. *Palaeogeography, Palaeoclimatology, Palaeoecology*, *254*(3–4), 561–582. <https://doi.org/10.1016/j.palaeo.2007.07.009>
- Wang, C. W., Hong, H. L., Li, Z. H., Yin, K., Xie, J., Liang, G. J., et al. (2013). The Eocene–Oligocene climate transition in the Tarim Basin, Northwest China: Evidence from clay mineralogy. *Applied Clay Science*, *74*, 10–19. <https://doi.org/10.1016/j.clay.2012.09.003>
- Wang, C. W., Hong, H. L., Song, B. W., Yin, K., Li, Z. H., Zhang, K. X., & Ji, J. L. (2011). The early-Eocene climate optimum (EECO) event in the Qaidam basin, northwest China: Clay evidence. *Clay Minerals*, *46*(04), 649–661. <https://doi.org/10.1180/claymin.2011.046.4.649>
- Weaver, C. E. (1984). *Shale-slate metamorphism in southern Appalachians*. Amsterdam: Elsevier.
- West, A. J., Galy, A., & Bickle, M. (2005). Tectonic and climatic controls on silicate weathering. *Earth and Planetary Science Letters*, *235*(1–2), 211–228. <https://doi.org/10.1016/j.epsl.2005.03.020>
- Wronkiewicz, D. J., & Condie, K. C. (1987). Geochemistry of archean shales from the Witwatersrand supergroup, South Africa: Source-area weathering and provenance. *Geochimica et Cosmochimica Acta*, *51*(9), 2401–2416. [https://doi.org/10.1016/0016-7037\(87\)90293-6](https://doi.org/10.1016/0016-7037(87)90293-6)
- Xiao, G. Q., Guo, Z. T., Dupont-Nivet, G., Lu, H. Y., Wu, N. Q., Ge, J. Y., et al. (2012). Evidence for northeastern Tibetan Plateau uplift between 25 and 20 Ma in the sedimentary archive of the Xining Basin, northwestern China. *Earth and Planetary Science Letters*, *317*–318, 185–195. <https://doi.org/10.1016/j.epsl.2011.11.008>
- Xiong, S. F., Ding, Z. L., Zhu, Y. J., Zhou, R., & Lu, H. J. (2010). A~ 6 Ma chemical weathering history, the grain size dependence of chemical weathering intensity, and its implications for provenance change of the Chinese loess–red clay deposit. *Quaternary Science Reviews*, *29*(15–16), 1911–1922. <https://doi.org/10.1016/j.quascirev.2010.04.009>
- Xiong, Y. (1986). *Soil map of China [in Chinese]*. Beijing: Geographic Publishing House.
- Yan, X. L., Miao, Y. F., Zan, J. B., Zhang, W. L., & Wu, S. (2014). Late Cenozoic fluvial–lacustrine susceptibility increases in the Linxia Basin and their implications for Tibetan Plateau uplift. *Quaternary International*, *334*, 132–140. <https://doi.org/10.1016/j.quaint.2013.12.046>
- Yang, R. S., Fang, X. M., Meng, Q. Q., Zan, J. B., Zhang, W. L., Deng, T., et al. (2017). Paleomagnetic constraints on the middle Miocene–early Pliocene stratigraphy in the Xining Basin, NE Tibetan Plateau, and the geologic implications. *Geochemistry, Geophysics, Geosystems*, *18*, 3741–3757. <https://doi.org/10.1002/2017GC006945>
- Yang, Y. B., Fang, X. M., Galy, A., Jin, Z. D., Wu, F. L., Yang, R. S., et al. (2016). Plateau uplift forcing climate change around 8.6 Ma on the northeastern Tibetan Plateau: Evidence from an integrated sedimentary Sr record. *Palaeogeography, Palaeoclimatology, Palaeoecology*, *461*, 418–431. <https://doi.org/10.1016/j.palaeo.2016.09.002>
- Yang, Y. B., Fang, X. M., Li, M. H., Galy, A., Koutsodendrakis, A., & Zhang, W. L. (2015). Paleoenvironmental implications of uranium concentrations in lacustrine calcareous clastic–evaporite deposits in the western Qaidam Basin. *Palaeogeography, Palaeoclimatology, Palaeoecology*, *417*, 422–431. <https://doi.org/10.1016/j.palaeo.2014.10.002>
- Yang, Y. B., Galy, A., Fang, X. M., Yang, R. S., Zhang, W. L., & Zan, J. B. (2017). Eolian dust forcing of river chemistry on the northeastern Tibetan Plateau since 8 Ma. *Earth and Planetary Science Letters*, *464*, 200–210. <https://doi.org/10.1016/j.epsl.2017.02.009>
- Ye, C. C., Yang, Y. B., Fang, X. M., Hong, H. L., Wang, C. W., Yang, R. S., & Zhang, W. L. (2018). Chlorite chemical composition change in response to the Eocene–Oligocene climate transition on the northeastern Tibetan Plateau. *Palaeogeography Palaeoclimatology Palaeoecology*, *512*, 23–32. <https://doi.org/10.1016/j.palaeo.2018.03.014>

- Ye, C. C., Yang, Y. B., Fang, X. M., & Zhang, W. L. (2016). Late Eocene clay boron-derived paleosalinity in the Qaidam Basin and its implications for regional tectonics and climate. *Sedimentary Geology*, *346*, 49–59. <https://doi.org/10.1016/j.sedgeo.2016.10.006>
- Zachos, J., Pagani, M., Sloan, L., Thomas, E., & Billups, K. (2001). Trends, rhythms, and aberrations in global climate 65 Ma to present. *Science*, *292*(5517), 686–693. <https://doi.org/10.1126/science.1059412>
- Zan, J. B., Fang, X. M., Yan, M. D., Zhang, W. L., & Lu, Y. (2015). Lithologic and rock magnetic evidence for the Mid-Miocene Climatic Optimum recorded in the sedimentary archive of the Xining Basin, NE Tibetan Plateau. *Palaeogeography, Palaeoclimatology, Palaeoecology*, *431*, 6–14. <https://doi.org/10.1016/j.palaeo.2015.04.024>
- Zan, J. B., Kang, J., Yan, M. D., Fang, X. M., Li, X. J., Guan, C., et al. (2018). A pedogenic model for the magnetic enhancement of late Miocene fluvial-lacustrine sediments from the Xining Basin, NE Tibetan Plateau. *Journal of Geophysical Research: Solid Earth*, *123*, 6176–6194. <https://doi.org/10.1029/2018JB016064>
- Zeng, L., Wang, L. S., Xu, H. X., Jiao, G. N., Cui, S. N., Han, H., & Zhang, B. S. (2010). *SY/T 5163-2010, Analysis Method for Clay Minerals and Ordinary Non-clay Minerals in Sedimentary Rocks by the X-ray Diffraction [in Chinese]* (). Beijing: Petroleum Industry Publishing House.
- Zhang, C. X., & Guo, Z. T. (2014). Clay mineral changes across the Eocene–Oligocene transition in the sedimentary sequence at Xining occurred prior to global cooling. *Palaeogeography, Palaeoclimatology, Palaeoecology*, *411*, 18–29. <https://doi.org/10.1016/j.palaeo.2014.06.031>
- Zhang, C. X., Xiao, G. Q., Guo, Z. T., Wu, H. B., & Hao, Q. Z. (2015). Evidence of late early Miocene aridification intensification in the Xining Basin caused by the northeastern Tibetan Plateau uplift. *Global and Planetary Change*, *128*, 31–46. <https://doi.org/10.1016/j.gloplacha.2015.02.002>
- Zhang, J., Wang, Y. N., Zhang, B. H., & Zhang, Y. P. (2016). Tectonics of the Xining Basin in NW China and its implications for the evolution of the NE Qinghai-Tibetan Plateau. *Basin Research*, *28*(2), 159–182. <https://doi.org/10.1111/bre.12104>
- Zhang, R., Jiang, D. B., Zhang, Z. S., & Yu, E. T. (2015). The impact of regional uplift of the Tibetan Plateau on the Asian monsoon climate. *Palaeogeography Palaeoclimatology Palaeoecology*, *417*, 137–150. <https://doi.org/10.1016/j.palaeo.2014.10.030>
- Zhang, W. F., Chen, J., Ji, J. F., & Li, G. J. (2016). Evolving flux of Asian dust in the north pacific ocean since the late Oligocene. *Aeolian Research*, *23*, 11–20. <https://doi.org/10.1016/j.aeolia.2016.09.004>
- Zhang, W. L., Zhang, T., Song, C. H., Appel, E., Mao, Z. Q., Fang, Y. H., et al. (2017). Termination of fluvial-alluvial sedimentation in the Xining basin, NE Tibetan Plateau, and its subsequent geomorphic evolution. *Geomorphology*, *297*. <https://doi.org/10.1016/j.geomorph.2017.09.008>, 86–99.
- Zhang, Z. S., Wang, H. J., Guo, Z. T., & Jiang, D. B. (2007). What triggers the transition of palaeoenvironmental patterns in China, the Tibetan Plateau uplift or the Paratethys Sea retreat? *Palaeogeography, Palaeoclimatology, Palaeoecology*, *245*(4), 317–331. <https://doi.org/10.1016/j.palaeo.2006.08.003>
- Zheng, D. W., Clark, M. K., Zhang, P. Z., Zheng, W. J., & Farley, K. A. (2010). Erosion, fault initiation and topographic growth of the north Qilian Shan (northern Tibetan Plateau). *Geosphere*, *6*(6), 937–941. <https://doi.org/10.1130/GES00523.1>
- Zheng, D. W., Zhang, P. Z., Wan, J. L., Li, C. Y., & Cao, J. X. (2003). Late Cenozoic deformation subsequence in northeastern margin of Tibet—Detrital AFT records from Linxia Basin. *Science in China, Series D: Earth Sciences*, *46*, 266–275. <https://doi.org/10.1360/03dz0021>
- Zheng, D. W., Zhang, P. Z., Wan, J. L., Yuan, D. Y., Li, C. Y., Yin, G. M., et al. (2006). Rapid exhumation at ~ 8 Ma on the Liupan Shan thrust fault from apatite fission-track thermochronology: Implications for growth of the northeastern Tibetan Plateau margin. *Earth and Planetary Science Letters*, *248*(1-2), 198–208. <https://doi.org/10.1016/j.epsl.2006.05.023>
- Zhuang, G. S., Hourigan, J. K., Koch, P. L., Ritts, B. D., & Kent-Corson, M. L. (2011). Isotopic constraints on intensified aridity in central Asia around 12 Ma. *Earth and Planetary Science Letters*, *312*(1–2), 152–163. <https://doi.org/10.1016/j.epsl.2011.10.005>